JOURNAL OF PROPULSION AND POWER
Vol. 30, No. 2, March–April 2014



# Powerplant Design and Performance Analysis of a Manned All-Electric Helicopter

Anubhav Datta*
*Science and Technology Corporation, Moffett Field, California 94035*
and
Wayne Johnson†
*NASA Ames Research Center, Moffett Field, California 94035*

DOI: 10.2514/1.B34843

**This paper describes the conceptual design of three all-electric powerplants — a battery-only, a fuel-cell-only, and a battery–fuel cell hybrid powerplant — for a manned ultralight utility helicopter (Robinson R 22 Beta II-like) and carries out a comparative evaluation of performance delivered by each. The new powerplants consist of a combination of high-pressure proton exchange membrane fuel cells, 700 bar type-4 hydrogen storage, a compressor–expander, lithium-ion batteries, and an alternating current synchronous permanent magnet motor. The key conclusion is that a hybrid powerplant that combines high specific power of batteries in hover and high calorific value of hydrogen in cruise delivers a superior performance compared to either system alone. The efficiency is higher than current rotorcraft piston engines but the key limitation is its low specific power, which is half of the current engines. Only 60% of the original payload can be flown (90 kg solo pilot) for a duration of 35 min (including 11 min hover) over a range of 47 km under high/hot (4000 ft/95°F) conditions. The paper lays the foundations of performance analysis for all-electric rotorcraft, benchmarks the best performance achievable with current state of the art, and quantifies future technology targets to enable performance comparable to existing internal combustion engines.**



## Nomenclature

| | | |
|---|---|---|
| $A$ | = | stack area, cm$^2$ |
| $E_h$, $E_r$ | = | ideal and practical reversible cell voltages, V |
| $F$ | = | Faraday constant, C/mol |
| $I$, $I_D$ | = | current, design current, A |
| $i$, $i_c$ | = | fuel cell current densities (nominal, design), A/cm$^2$ |
| $k$ | = | battery Peukart coefficient |
| $L_S$ | = | stack volume, L |
| $m_{\mathrm{H/O/A}}$ | = | molecular masses of hydrogen, oxygen, and air, kg/mol |
| $\dot{m}_{\mathrm{H},S}$, $\dot{m}_{\mathrm{O},S}$, $\dot{m}_{\mathrm{A},S}$ | = | supply rates of hydrogen, oxygen, and air, mol/s |
| $n_c$ | = | number of cells |
| $P$, $P_D$, $P_{\max}$ | = | power, design power, maximum power, kW |
| $p$, $p_c$, $p_{\max}$ | = | fuel cell power densities (nominal, design, maximum), W/cm$^2$ |
| $Q$ | = | motor torque, Nm |
| $\dot{Q}$ | = | heating rate, kW |
| $r$ | = | battery internal resistance, Ω |
| $S_{\mathrm{H}}$, $S_{\mathrm{O}}$ | = | hydrogen and oxygen stoichiometries |
| $t_c$ | = | fuel cell effective thickness, cm |
| $V$ | = | voltage, V |
| $V_{\mathrm{br}}$, $V_{\mathrm{be}}$ | = | speeds for best range and best endurance, km/h |
| $v$, $v_c$ | = | fuel cell voltages (nominal, design), V |
| $W_S$ | = | stack weight, kg |
| $\dot{w}_{\mathrm{H},S}$, $\dot{w}_{\mathrm{O},S}$, $\dot{w}_{\mathrm{A},S}$ | = | supply rates of hydrogen, oxygen, and air, kg/s |
| $x$ | = | battery depth of discharge fraction |
| $x_{\mathrm{O}}$ | = | mole fraction of oxygen in dry air |
| $\eta_f$, $\eta_H$, $\eta_M$ | = | efficiencies; stack, fuel, and motor |
| $\lambda_{\mathrm{H}}$, $\lambda_{\mathrm{A}}$ | = | effective stoichiometries of hydrogen and air |
| $\xi$ | = | fuel cell porosity fraction |
| $\rho$ | = | hydrogen density, kg/L |
| $\rho_c$ | = | fuel cell effective density, kg/m$^3$ |

Presented as Paper 2012-5405 at the 12th AIAA Aviation Technology, Integration, and Operations (ATIO) Conference and 14th AIAA/ISSMO Multidisciplinary Analysis and Optimization Conference, Indianapolis, IN, 17–19 September 2012; received 6 November 2012; revision received 11 February 2013; accepted for publication 4 June 2013; published online 20 February 2014. 

*Rotorcraft Dynamicist, NASA Ames Research Center. Senior Member AIAA.
†Aeromechanics Branch. Fellow AIAA.

## I. Introduction

THIS paper describes the conceptual design of all-electric powerplants for a manned ultralight utility helicopter and carries out a systematic performance analysis in hover and cruise flight. The objectives are to assess the current status of technology in all-electric aviation and determine future technology targets needed to achieve performance comparable to combustion engines. This research is part of a broad vision for sustainable aviation that will reduce dependency on hydrocarbon fuels, eliminate pollutants and greenhouse gas emissions, and contribute to the global energy related carbon dioxide target of 50% below current by the year 2050. To this end, the paper explores a fundamental transformation of a rotorcraft propulsion system — fuel, storage, and engine — beginning at the ultralight range.

Reducing dependency on hydrocarbon fuels will require a complete overhaul of all energy flow segments: production, transfer, storage, and extraction. Sustainable production and transfer are already being addressed in the context of electric vehicles (EVs) and plug-in hybrid electric vehicles (HEVs) [1]. Storage and extraction based on electrochemical sources and electric motors are a major thrust area in the automobile industry. Electric vehicles driven by batteries are now becoming commercially available with increasing energy capacities; for example, the Chevrolet Volt (16 kWh), Ford Focus (23 kWh) and Nissan Leaf (24 kWh). Electric vehicles driven by fuel cells are also making their debut with increasing power ratings; for example, the Audi Q5 (93 kW), the Honda Clarity 2009 (100 kW), and the Mercedes F125 (172 kW). In the U.S., the ongoing Department of Energy's (DOE's) Hydrogen Program (HP) [2] is focused on achieving specific hydrogen and fuel cell technology targets for storage and extraction in light utility vehicles by the year 2015. Even though the specific energy and power of these systems still fall far short for purposes of practical aviation, significant advances over the last decade begin to make a case

for their detailed assessment. The intent of this paper is to carry out such an assessment.

In fixed-wing aviation, a manned all-electric battery–fuel cell hybrid demonstrator aircraft was flown successfully by Boeing in 2008 by converting a two-seat Austrian HK36 motor glider of 700 kg gross takeoff weight (GTOW) [3,4] with a supply of around 30 kW of power. In rotary-wing aviation, the requirements of hover and low-speed flight translate into very high specific power, energy, and torque requirements that are unique and usually far more stringent than other aeronautical applications. Inventors have over the last two years begun successful demonstrations of manned all-electric rotorcraft flight [5,6] using batteries. These take advantage of innovative bare-bones airframes to reduce power required rather than improve electric powerplant to increase power supplied, and are all limited to around 5–10 min of flight. An effort to demonstrate an all-electric (battery) helicopter of practical relevance is currently underway in Sikorsky (project Firefly) using a S-300C helicopter of 930 kg GTOW as a conversion baseline. A major challenge for this battery-powered rotorcraft is once again its anticipated low endurance of around 15 min. The focus of this paper is on rotary-wing aviation and, in particular, on proposing alternatives to increase the range and endurance of all-electric propulsion.

The propulsion system explored in this paper is a hybrid of proton exchange membrane fuel cells (PEMFC) and lithium-ion batteries, in addition to each system alone. The hybrid system uses the advantage of each: high energy of hydrogen fuel to extend range and endurance and high power of lithium-ion batteries to maintain hover ceiling. It is motivated by the Honda automobile [7,8] (fuel cells and supercapacitor) and the Boeing airplane [3,4] (fuel cell and batteries) but applied here in the context of rotary-wing aircraft. The approach is to begin with an ultralight utility helicopter model as baseline (the Robinson R 22 Beta II-like), replace its existing piston engine with the all-electric powerplant models, and carry out detailed performance studies on the converted aircraft. Recently, conceptual studies have begun to appear on the design of direct drive electric powertrains for this helicopter [9,10]. The emphasis of this paper is on the powerplant — its design and evaluation, a systematic assessment of the aircraft performance, and a documentation of future requirements based on performance targets.

The paper is organized as follows. Following the Introduction, Sec. II summarizes the baseline aircraft and its analysis. Section III describes the preliminary design of the five major components of the new powerplants, including a survey of the current state of the art in each. Section IV synthesizes three types of powerplants — a battery-only (B-only), a fuel-cell-only (FC-only), and a battery–fuel cell hybrid (BFC-hybrid) powerplant — using the building blocks described in Sec. III. These powerplants are then sized and characterized in terms of engine performance. Section V studies the performance of the converted all-electric aircraft. Three benchmark missions are proposed. Section VI summarizes the current state of technology relative piston engines. Based on this summary and the preliminary design and survey carried out in Sec. III, future technology requirements are listed. Section VII concludes the paper with four major conclusions from this work.

## II. Baseline Helicopter

The two-seat Robinson R22 Beta II helicopter (Fig. 1) is considered as baseline. It is one of the world's largest selling light-utility helicopters, the counterpart of Cessna 172 in the fixed-wing world. The relevant specifications available in the public domain are as follows. They are assumed to be at Sea Level/International Standard Atmosphere (SL/ISA, i.e., 1 atm, 59°F or 15°C).

*Aircraft*: Maximum GTOW = 622 kg; empty weight = 388 kg; maximum payload(PL) = 2 people + baggage = 181 kg (standard) and 153 kg (with auxiliary tank); rotor speed = 510 rpm; cruise speed (at 70% power) = 177 km/h; economical cruise speed = 153 km/h; endurance (at 65% power) = 3 h 20 min (but corresponding PL unknown); range = 333 km (standard) and 555 km (with auxiliary tank).

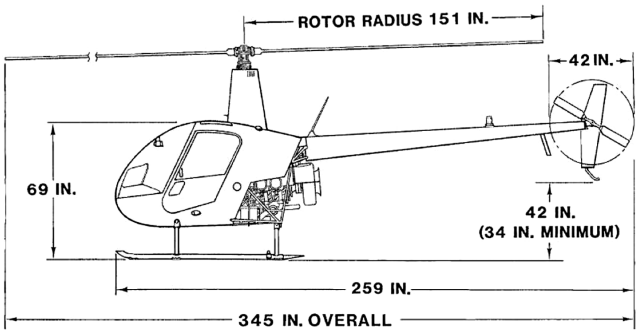


**Fig. 1 The two-seat Robinson R22 Beta II helicopter.**

*Engine*: One Lycoming O-360-J2A engine; maximum derated power = 97.5 kW (transmission limit); continuous operating power = 93 kW (at maximum speed); cruise power (assumed 70% of derated) = 68.25 kW; endurance power (assumed 65% of derated) = 63.4 kW; engine speed = 2652 rpm; weight (dry) = 117 kg; volume = 362 L.

*Fuel*: Maximum fuel weight = 52 kg (standard) + 29 kg (auxiliary) = 81 kg; fuel volume = 72.5 L (standard) + 39.75 L (auxiliary) = 112.25 L; tank weight unknown, 5% fuel weight (assumed) = 2.6 kg (standard) + 1.45 kg (auxiliary) = 4.05 kg; tank volume assumed included in fuel volume.

The power required to fly the aircraft is predicted based on standard analysis procedures [11] carried out using the University of Maryland Advanced Rotorcraft Code [12] using simple models (in absence of detailed rotor and fuselage data) modified appropriately with guidance from the pilot's operating handbook [13] to reproduce gross performance characteristics given earlier. The model considers rigid blade structures (flap and torsion only), blade element aerodynamics (two-dimensional airfoil tables, quasi-steady aerodynamics, and uniform inflow), and propulsive trim with lookup table based aircraft properties. For example, Fig. 2 shows typical aircraft power predictions for varying GTOW under SL/ISA. There are no data available for validation; instead, airfoil zero-angle drag and fuselage drag are set appropriately to reproduce hover power and forward flight best range speed $V_{br}$.

## III. Conceptual Design of All-Electric Powerplant

The electric powerplant consists of five major components: a PEMFC system, a compressor–expander (C–E), hydrogen storage, lithium-ion batteries, and a main electric motor (Fig. 3 is a block diagram of the notional configuration). The fuel cell and the battery pack are connected to the main bus in parallel via regulators (guided by [3]), which then connects to the transmission via the motor. The conceptual design of the major components are described next with

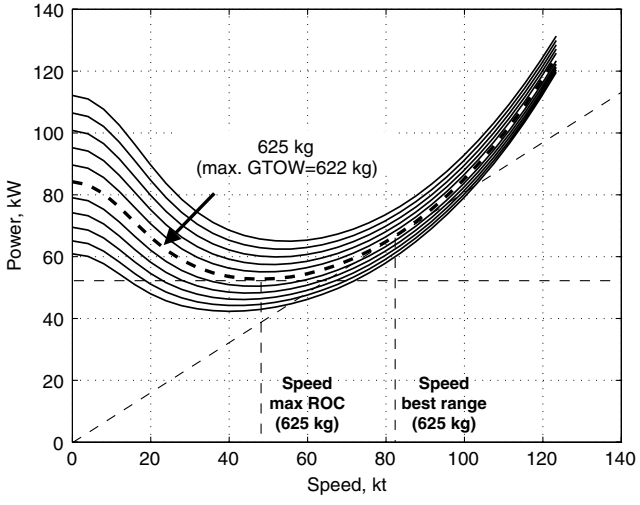


**Fig. 2 Predicted power versus speed at SL/ISA for various GTOW.**

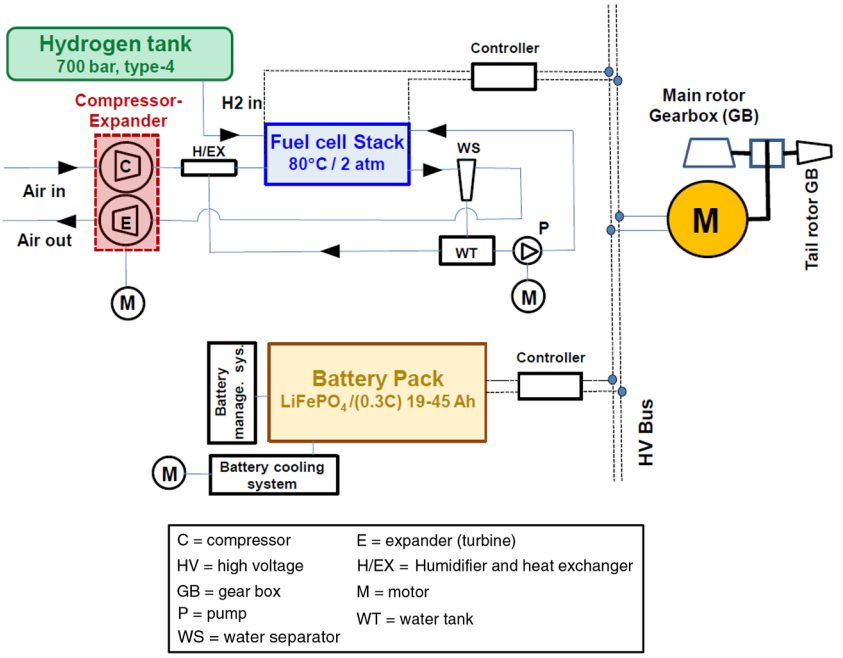


**Fig. 3 Major components of a hybrid battery fuel cell power system.**



emphases on the state of the art in each and challenges related to the present application.

### A. PEMFC system

The preliminary design of the PEMFC system follows textbook procedures [14–16]. PEMFC has the highest specific power of all fuel cells today and is, therefore, considered the basis for the present design. A fuel cell system includes the stack, balance of plant (BOP), fuel system, and power electronics. The BOP includes air, thermal, and water management systems. Out of all BOP components, the C–E of the air management system is particularly heavy but important for altitude losses and is, hence, considered in detail.

#### 1. *Stacks*

The typical current–voltage ($i$-$v$) characteristics of a PEMFC are shown in Fig. 4a (data from [17]). The corresponding power–voltage ($p$-$v$, where $p = iv$) characteristics are shown in Fig. 4b. Operations at 2 to 3 atm are considered for the current design. Static models are fit to the data [16] for smooth variations during design trade studies. High-voltage operation (left side of curves) minimizes fuel weight, low-voltage operation (right side of curves) minimizes stack weight. For a required power output $P_D$ at a voltage $V_D$, the choice of the design (or rated) cell voltage $v_c$ sizes the stack. Then, the number of cells in the stack must equal $n_c = V_D/v_c$. The rated cell current density $i_c$ and power density $p_c = i_c v_c$ are then determined by the characteristic curves. The rated current drawn from the stack is $I_D = P_D/V_D = P_D/(n_c v_c)$. The stack active area is then given by $A = I_D/i_c = P_D/(n_c v_c i_c) = P_D/(n_c p_c)$. Once the stack design conditions are set (i.e., $n_c$ and $A$ set to produce $P_D$ at $V_D$ at an operating $v_c$), the output current, voltage, and power are set by controlling the cell current density $i$,

$$I = Ai; \qquad V = n_c v; \qquad P = VI = An_c p \tag{1}$$

where $v$ and $p$ are obtained corresponding to $i$ from the characteristic curves. The cell current $i$ is related to the fuel flow rate (the current is controlled by a converter and the fuel and air flows are adjusted to maintain the required utilization). The maximum power available from the stack is $P_{\max} = An_c p_{\max}$, where $p_{\max}$ is the maximum cell power density. The stack efficiency $\eta_f = v/E_h$ where $E_h = 1.472$ V is the ideal reversible cell voltage corresponding to the enthalpy of formation (heating value) of the reaction $H_2 + (1/2)O_2 \rightarrow H_2O(l)$ at 80°C, pure reactants at 1 atm, and product water in liquid form (i.e., higher heating value). Note that the practical reversible cell voltages $E_r$ using impure reactants (air instead of oxygen) and operating at pressures of 2 and 3 atm are 1.180 and 1.176 V, respectively, but are not used for quoting efficiencies. The practical irreversible cell voltage is $v$, which varies as per the $i$-$v$ plots shown earlier.

Consider a stack designed to deliver $P_D = 81.33$ kW at voltage $V_D = 250$ V. Let the operating pressure be 2 atm. (The maximum

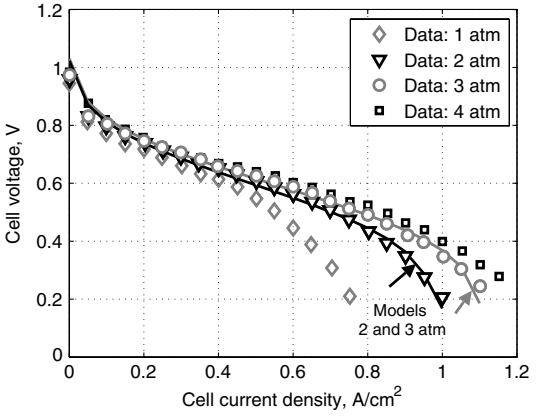


**a) Current density versus voltage ($i$-$v$)**

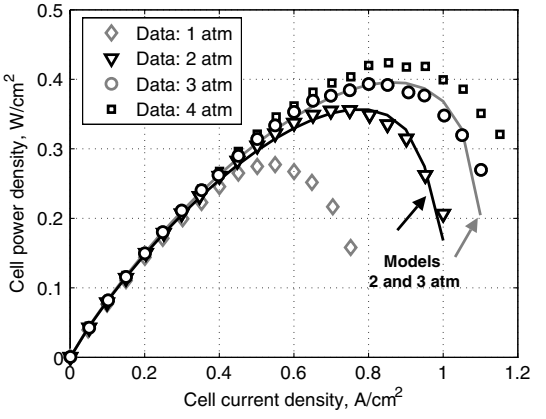


**b) Power density versus voltage ($p$-$v$)**

**Fig. 4 Typical characteristics of a single PEMFC fuel cell.**

net power from such a stack equals the maximum power required by the helicopter, as shown later.) Depending on the choice of $v_c$, the resulting stack will have one of the operating characteristics shown in Fig. 5. The plot shows the gross power from the stacks. A part of this power will be used for the compressor required to achieve the high operating pressure. Compression to 3 atm obviously takes more power than to 2 atm, particularly due to the additional pressure loss with altitude. Thus, a 2 atm operation provides a greater percentage of gross power as net power (net % useful) or effective power (kWe). It also implies a smaller compressor. An estimate of the stack volume and weight is made using

$$L_S = n_c A t_c = \frac{P_D}{p_c} t_c = \frac{P_{\max}}{p_{\max}} t_c; \qquad W_S = L_S \rho_c \xi \tag{2}$$

where $t_c$ is the average thickness of an individual cell unit, including the membrane electrode assembly, catalysts, and flow structure; $\rho_c$ is the average density of the individual cell unit; and $\xi$ is its porosity, ≈0.6. Thus, the stack is sized only by the power output and the cell power density. The output voltage determines only the configuration of stack (number of cells $n_c$ and active area $A$) but not the weight or volume. An estimate of the material properties ($t_c$ and $\rho_c$) is made using Honda Clarity 2009 fuel cell car data [8]: $P_{\max} = 100$ kW, $L_S = 57$ L (power density 1.75 kW/L), and $W_S = 68$ kg (specific power 1.47 kW/kg). The stack operating characteristics are not known, and so, for conservative estimates, it is assumed to behave as the 3 atm characteristics (higher than 3 atm is unlikely). Thus, $p_{\max}$ is obtained from the 3 atm $i$-$v$ curve. Using a porosity of $\xi = 0.6$, we have $t_c = 2.224$ mm and $\rho_c = 1988$ kg/m$^3$. Porosity is merely a scaling factor and does not affect final weights. The stack size then varies with the design cell voltage $v_c$, as shown in Fig. 6.

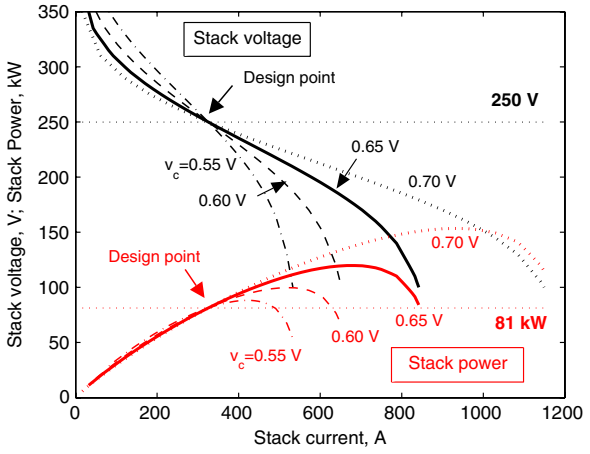


**Fig. 5 Stack voltage and power versus current; rated power 81 kW, voltage 250 V.**

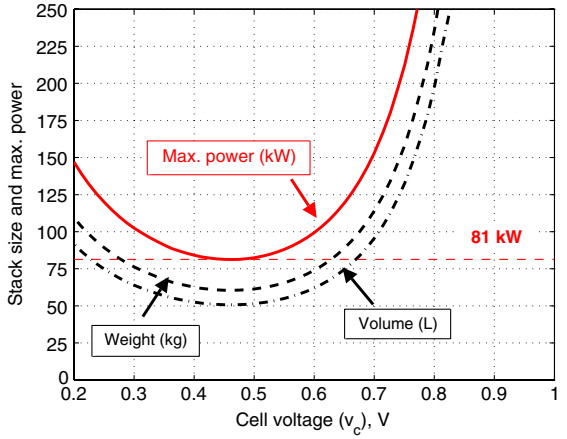


**Fig. 6 Stack size and maximum power versus choice of design operating cell voltage $v_c$; rated power 81 kW.**

**Table 1 Four stack designs; stack temperature 80°C and hydrogen/air stoichiometry 1/2.5; operations at SL/ISA**

| Parameters | S2.98 | S2.68 | S3.98 | S3.68 |
|---|---|---|---|---|
| Pressure, atm | 2 | 2 | 3 | 3 |
| $P_{\text{rated}}$, kW | 81.33 | 56.30 | 93.25 | 64.55 |
| $P_{\text{net}}$, kWe | 69.2 | 47.9 | 72.7 | 50.3 |
| Net useful power, % | 85.1 | 85.1 | 78.0 | 78.0 |
| $P_{\text{max net}}$, kWe | 97.5 | 67.5 | 97.5 | 67.5 |
| Maximum net useful power, % | 81.4 | 81.4 | 71.2 | 71.2 |
| Number of cells | 384 | 384 | 384 | 384 |
| A, cm$^2$ | 875 | 606 | 901 | 624 |
| $v_c$, V | 0.651 | 0.651 | 0.651 | 0.651 |
| $i_c$, A/cm$^2$ | 0.372 | 0.372 | 0.414 | 0.414 |
| $I_D$, A | 325 | 225 | 373 | 258 |
| $V_D$, V | 250 | 250 | 250 | 250 |
| $\eta_f$ | 0.44 | 0.44 | 0.44 | 0.44 |
| $Q$, kW | 102.8 | 71.1 | 117.7 | 81.5 |
| $W_S$, kg | 89.15 | 61.71 | 91.81 | 63.56 |
| $L_S$, L | 74.74 | 51.74 | 76.97 | 53.28 |

The choice of $v_c \approx 0.45$ V maximizes power density $p_c$ (Figs. 4a and 4b) and produces the minimum size. The maximum power, however, is limited to exactly 81.33 kW. A higher $v_c = 0.65$ V produces a larger stack, but also delivers a maximum power of 119.73 kW. This margin is needed to provide BOP and other expenses. The net power, or effective power (kWe), is gross power minus these expenses. Note that a higher $v_c$ also increases stack efficiency ($\eta_f = v_c/E_h$), meaning less fuel and less waste heat. A cell voltage of $v_c = 0.65$ V is chosen for the current design. This gives $L_S = 74.74$ L (energy density 1.6 kW/L) and $W_S = 89.15$ kg (specific energy 1.34 kW/kg). As reference, DOE 2015 targets for power density and specific power are 2 kW/L and 2 kW/kg, respectively, for a reference stack of 80 kWe maximum net power (gross power minus BOP expenses and other losses).

Table 1 shows four stack designs, two each for 2 and 3 atm operations, one for high power, and one for low power. The high and low powers correspond to maximum net powers of 97.5 and 67.5 kWe, respectively. The 97.5 kWe stack is meant for a fuel-cell-only powerplant. The 67.5 kWe stack is meant for a battery–fuel cell hybrid powerplant, where 30 kW is delivered by the battery. The BOP loss is the compressor loss. Other accessories are assumed to consume 5% of rated power. Two or three stack modules may be used in parallel to achieve the required stack area.

### 2. *Fuel Flow*

The electrode half reactions are

$$H_2 \rightarrow 2H^+ + 2e^- \text{ anode, release of electrons, oxidation}$$

$$(1/2)O_2 + 2e^- + 2H^+ \rightarrow H_2O \text{ cathode,}$$

capture of electrons, reduction

From elementary chemistry, to produce a current $I$, hydrogen consumption rates must equal $\dot{m}_{H,C}$ mol/s or $\dot{w}_{H,C}$ kg/s where

$$\dot{m}_{H,C} = S_H \frac{1}{NF} I n_c = S_H \frac{1}{NF} \frac{P}{v}; \qquad \dot{w}_{H,C} = m_H \dot{m}_{H,C} \tag{3}$$

Here, $S_H = 1$ is hydrogen stoichiometry (see anode reaction), $N = 2$ is number of electrons participating, $F = 96485$ C/mol is the Faraday constant, and $m_H = 2.016 \times 10^{-3}$ kg/mol is the molar mass of hydrogen. Supply rate is consumption rate divided by the fuel efficiency factor $\eta_H$. The effective stoichiometry is then $\lambda_H = S_H/\eta_H$. Hydrogen is expensive, hence, typically $\eta_H \approx 1$, i.e., $\lambda_H \approx S_H$. The hydrogen supply rate depends only on the power output and the cell voltage. Given a fixed power output and cell voltage, the total time of operation is simply the amount of hydrogen available divided by the supply rate. Figure 7 shows the power versus time of operation. Increase in cell voltage increases stack efficiency and, hence, amount of energy extracted from hydrogen. Thus, it is desirable to have as

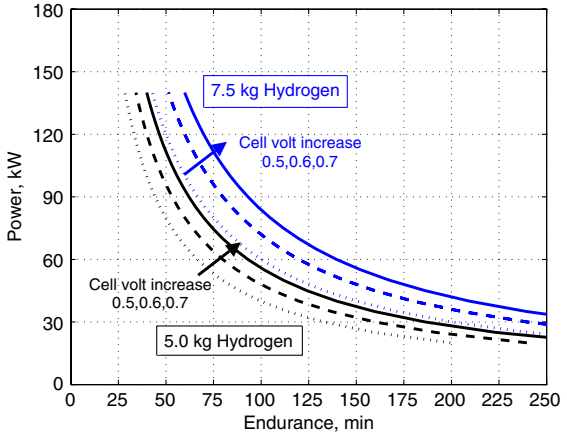


**Fig. 7 Power versus time of operation for 5 and 7.5 kg of hydrogen and various cell voltages.**

high a cell voltage as possible. This is in direct contradiction to cell voltage desired for minimum stack weight (Fig. 6). The oxygen consumption and the air supply rates are

$$\dot{w}_{O,C} = S_O \frac{m_O}{NF}\frac{P}{v}; \qquad \dot{w}_{A,S} = \lambda_A \frac{m_A}{x_O NF}\frac{P}{v} \tag{4}$$

Here, $m_O = 32 \times 10^{-3}$ kg/mol is the molecular mass of oxygen, $S_O = 1/2$ is oxygen stoichiometry (see cathode reaction), $m_A = 28.97 \times 10^{-3}$ kg/mol is the molecular mass of air, and $x_O = 0.2095$ is the mole fraction of oxygen in dry air. For PEMFC, it is required that effective stoichiometry be at least $\lambda_A \approx 2.5 S_O$. The air supply rate minus the oxygen consumption rate is the air exhaust rate. The hydrogen consumption rate plus the oxygen consumption rate is the water exhaust rate. The latter is in combined liquid and vapor form. The individual contents are calculated based on a stack pressure drop (assumed 0.3 atm), the saturated vapor pressure of water at the operating temperature 80°C, and assuming exit pressure equals vapor pressure plus dry air pressure. The humidity ratio is the ratio of vapor exhaust rate to air exhaust rate. Table 2 shows the fuel flow rates for the four stacks at their rated powers. The endurance (for 5 kg of fuel) and capacity (rated power multiplied by endurance) are also shown for reference. The high-pressure operation requires a compressor. Depending on the stack operating pressure and internal pressure drop, an expander can be used at the exit to recover some of this power.

### 3. *Compressor–Expander*

A compressor is needed at the inlet of the stack to compress air from ambient pressure (ambient pressures at 7000 and 14,000 ft are 77 and 59% of SL pressure, respectively, for example) to stack operating pressure (2 or 3 atm). The compressor power is the main source of BOP and altitude losses. A part of this loss can be recovered using an expander (turbine) at the outlet of the stack. The expander outlet is at ambient pressure. The compressor and expander power are calculated using isentropic assumptions. Their efficiencies are assumed to be 60%.

The C–E weight is calibrated to an advanced unit built by Honeywell for a 80 kWe automotive fuel cell system for DOE HP in 2005 [18,19]. The input power for the C–E combined or compressor alone is estimated to be 9.4 or 15.7 kW for 2–3 atm operation. It assumes a hydrogen and air flow rate of 0.09 kg/s at full flow, outlet pressure of 2.5 atm, an expander inlet flow rate of 0.093 kg/s, and expander inlet conditions of 80°C and 2.2 atm. It weighs 11 kg and has a volume of 6.5 L. Typical performances achievable today are efficiencies of 70% for the compressor and 80% for the turbine, pressure ratios of 2.5 : 1, and flow rates of around 0.1 kg/s.

Table 3 shows the C–E specifications and sizes for the four stacks. The weight and volume are scaled to maximum flow rates (at SL/ISA), to be conservative in the absence of data, and, hence, show higher values than the Honeywell unit (e.g., 27.55 kg for a 97.5 kWe unit compared to Honeywell's 11 kg for a 80 kWe unit). The maximum flow rates depend on maximum power output, hence, stack pressure, and so a reduction in stack pressure leads to a reduction in C–E power as well as its size. Reduction in C–E power means an increase in net power output. From Tables 2 and 3, the low power stacks (S2.68 and S3.68) appear to be near the state of the art in terms of flow rates (0.0775, 0.0888 kg/s), whereas the high-power stacks (S2.98 and S3.98) are beyond. The greater C–E power loss at 3 atm more than offsets the advantage of improved $i$-$v$ characteristics and leads to a bigger stack for the same net power (Table 1). It also means a bigger C–E. Thus, 2 atm is considered as the operating pressure.

**Table 2 Fuel flow rates for four stack designs; humidity ratio = 0.24; endurance shown with 5 kg of hydrogen; capacity is rated power × endurance (remains same for a fixed amount of hydrogen)**

| Parameters | S2.98 | S2.68 | S3.98 | S3.68 |
|---|---|---|---|---|
| Hydrogen in, g/s | 1.31 | 0.90 | 1.50 | 1.04 |
| Air in, kg/s | 0.112 | 0.0775 | 0.128 | 0.0888 |
| Air in, L/m | 3359 | 2326 | 2568 | 1777 |
| Air out, kg/s | 0.102 | 0.0703 | 0.117 | 0.0806 |
| Vapor out, kg/s | 0.024 | 0.017 | 0.015 | 0.0105 |
| Endurance, m | 63.8 | 92.2 | 55.7 | 80.4 |
| Capacity, kWh | 86.5 | 86.5 | 86.5 | 86.5 |

## B. Hydrogen Storage

### 1. *Storage Tanks*

Hydrogen must be extracted from natural sources (by fossil fuel steam reformation or water electrolysis, which have their own carbon emission and efficiency issues that are beyond the scope of this paper) and stored onboard. The density at SL/ISA is $\rho_{H,ISA} = 8.525 \times 10^{-5}$ kg/L. The density increases under pressure; for example, $\rho_{H,350b} = 0.0229$ kg/L (350 bar/5000 psi, 21°C) and $\rho_{H,700b} = 0.0393$ kg/L (700 bar/10,000 psi, 21°C). The density of liquid hydrogen is yet higher, $\rho_{H,L} = 0.07099$ kg/L, but significant amounts of energy must be spent on liquefaction. Because its boiling point is −252.85°C, adequate insulation must be provided for cryogenic storage. For the present design, only gaseous hydrogen is considered.

The density of gasoline is $\rho_{gas} = 0.72$ kg/L. Thus, a kilogram of hydrogen stored even in liquid form takes 10 times more space than gasoline. The specific energy (also called gravimetric energy density or calorific value) varies between 33 and 39.4 kWh/kg depending on lower or higher heating values. In comparison, the gravimetric density of gasoline is almost one-third, 13 kWh/kg. Thus, a

**Table 3 Compressor–Expander operations corresponding to four stack designs; assumed stack pressure loss of 0.3 atm, efficiencies are 0.6 (T, temperature; P, Power; p, pressure)**

| Parameters | S2.98 | S2.68 | S3.98 | S3.68 |
|---|---|---|---|---|
| Compressor T in, °C | 15 | 15 | 15 | 15 |
| Compressor T out, °C | 120 | 120 | 192 | 192 |
| Compressor p in, atm | 1 | 1 | 1 | 1 |
| Compressor p out, atm | 2 | 2 | 3 | 3 |
| Compressor P, kW | 11.83 | 8.19 | 22.84 | 15.81 |
| Compressor P max, kW | 23.86 | 16.52 | 46.90 | 32.47 |
| Expander T in, °C | 80 | 80 | 80 | 80 |
| Expander T out, °C | 50.3 | 50.3 | 28.4 | 28.4 |
| Expander p in, atm | 1.7 | 1.7 | 2.7 | 2.7 |
| Expander p out, atm | 1 | 1 | 1 | 1 |
| Expander P, kW | −3.77 | −2.61 | −6.95 | −4.81 |
| Expander P max, kW | −7.61 | −5.27 | −14.26 | −9.87 |
| Net P, kW | 8.06 | 5.58 | 15.89 | 11.00 |
| Net P max, kW | 16.25 | 11.25 | 32.64 | 22.59 |
| Weight, kg | 27.55 | 19.07 | 32.15 | 22.26 |
| Volume, L | 16.26 | 11.25 | 18.98 | 13.14 |

**Table 4 Technology levels for some commercially available hydrogen storage tanks**

| Storage type | Company/model | $H_2$, kg | Tank weight, kg | Tank volume, L | Gravimetric, kg/kg | Volumetric, kg/L |
|---|---|---|---|---|---|---|
| 4 (350 bar) | QT[a]/109176 | 1.32 | 16.8 | 34 | 0.0786 | 0.0388 |
| 4 (350 bar) | QT/110500 | 1.55 | 20.0 | 40 | 0.0775 | 0.0388 |
| 4 (700 bar) | QT/110463 | 5.00 | 92.0 | 129 | 0.0543 | 0.0388 |
| 3 (350 bar) | DT[b]/W205 | 4.89 | 95.0 | 285 | 0.0515 | 0.0172 |
| 3 (350 bar) | DT/ZD154 | 3.73 | 82.0 | 231 | 0.0455 | 0.0161 |
| 3 (350 bar) | DT/ZM180 | 4.26 | 93.0 | 276 | 0.0458 | 0.0154 |
| 3 (450 bar) | DT/W076 | 2.17 | 53.6 | 137 | 0.0405 | 0.0158 |
| 3 (450 bar) | DT/W303 | 8.64 | 170.5 | 343.5 | 0.0507 | 0.0252 |

[a]Quantum Technologies
[b]Dynetek Industries, Ltd.

**Table 5 Technology levels for DOE Hydrogen Program estimated hydrogen storage based on 5.6 kg of stored hydrogen**

| Storage type | Gravimetric, kg/kg | Volumetric, kg/L |
|---|---|---|
| 3 (350 bar) | 0.042 | 0.0174 |
| 4 (350 bar) | 0.055 | 0.0176 |
| 3 (700 bar) | 0.036 | 0.0250 |
| 4 (700 bar) | 0.052 | 0.0263 |
| Liquid $H_2$ | 0.057 | 0.023 |
| Cryocompressed $H_2$ (steel shell) | 0.055 | 0.0411 |
| Cryocompressed $H_2$ (Al shell) | 0.090 | 0.0411 |
| 2010 target | 0.045 | 0.028 |
| 2015 target | 0.055 | 0.040 |
| Ultimate target | 0.075 | 0.070 |

kilogram of hydrogen stores around three times more energy than a kilogram of gasoline. This is the primary motivation for using hydrogen as fuel. The energy density (also called volumetric energy density) for gasoline, which is specific energy (gravimetric energy density) times density, is 9.36 kWh/L. The energy densities of hydrogen for 700 bar gas or liquid are 1.55 kWh/L and 2.8 kWh/L, respectively. Thus, compared to gasoline, a liter of gaseous hydrogen at 700 bar stores about one-sixth the energy and a liter of liquid hydrogen stores one-third the energy. These numbers, corresponding to hydrogen alone (without tank) define the theoretical upper limits for storage gravimetric and volumetric densities (with tank).

The technology levels for storage gravimetric and volumetric capacities; that is, a kilogram of hydrogen per kilogram of tank and a kilogram of hydrogen per liter of tank system, vary widely depending on the form of storage (compressed gas, cryogenic, cryocompressed, solid state), measured data or analysis predictions, small-scale laboratory demonstration or production level tanks, type and material of tank construction, and the actual amount of hydrogen stored. Table 4 shows compressed hydrogen storage data from commercial onboard tank producers. Only types 3 (metal liner) and 4 (nonmetal/plastic, high-density polyethylene liner) will be considered (types 1 and 2 are for storage pressures lower than 350 bar; used in buses but are too heavy and large for aviation). Type 3 tanks are those that have metal liners reinforced with filament wrapping. Type 4 tanks are more advanced, and have nonmetal/plastic liners with resin impregnated filament wrappings.

Table 5 shows analytical estimates for a variety of onboard storage systems from the DOE HP for 5.6 kg of hydrogen. Even though the DOE targets are meant to reflect requirements, not status of technology, these estimates are representative of what is achievable. The table shows that current technology meets earlier 2010 targets but falls short of 2015 targets in volumetric capacity. The ultimate targets for volumetric capacity are yet higher. The ultimate targets for gravimetric capacities are met today, but only for small quantities of hydrogen. Storage based on metal hydride and other solid-state technologies are not considered (poor gravimetric capacities at present). The present design is based on specifications of the type 4, 700 bar QT/110463 tank (Table 4), even though the hydrogen storage amounts considered will vary between 1.6 and 7.2 kg.

### 2. *Stack-Storage Combined System*

The design cell voltage is chosen considering the operation of the combined stack and storage system. A lower voltage lowers the stack weight (Fig. 6) but raises the fuel weight (Fig. 7) and vice versa. The tank and stack weights are not known a priori, and so the weight fraction of each is varied — from a heavy tank and a light stack to a light tank and a heavy stack — to obtain a Ragone plot that shows the range of specific power and energies possible from the combined system. The plot does not depend on the actual weight of the combined system, but only on the technology levels ($i$-$v$ characteristics, stack construction, and storage type) and operating conditions (cell voltage, anode/cathode humidity, and stack pressure). Intersection of this plot with an intended time of operation can then be used to determine optimum operating parameters. The final stack designs shown earlier were chosen based on this combined analysis.

The variation of specific power with specific energy for various design cell voltages is shown in Fig. 8. To generate the plots, fuel system weight fraction is varied from 10 to 90% (with corresponding stack weight fraction varied from 90 to 10%). A 700 bar type 4 hydrogen storage is considered. Clearly, the most suitable voltage depends on the intended time of operation. For a 15–60 min operation, 0.55 V is most suitable. For a 60 min to 2 h operation, 0.6 V is most suitable. Higher specific energy reduces specific power accordingly, but energy available from hydrogen being far superior to any other electrochemical device, maximizing energy should almost always be the target as long as the maximum power requirement is met. From Fig. 8, 0.60–0.65 V appears to be the most suitable operating voltage (minimum stack and storage weight) over a wide range (1–4 h) of operating time.

The effect of hydrogen storage technology is shown in Figs. 9a and 9b for 0.60 V design cell voltage (the plot for 0.65 V is similar). From Fig. 9a, it appears that, in terms of weight, all present storage types coalesce to a similar plot, whereas the DOE 2015 target requires a dramatic improvement. This improvement is essential for aviation

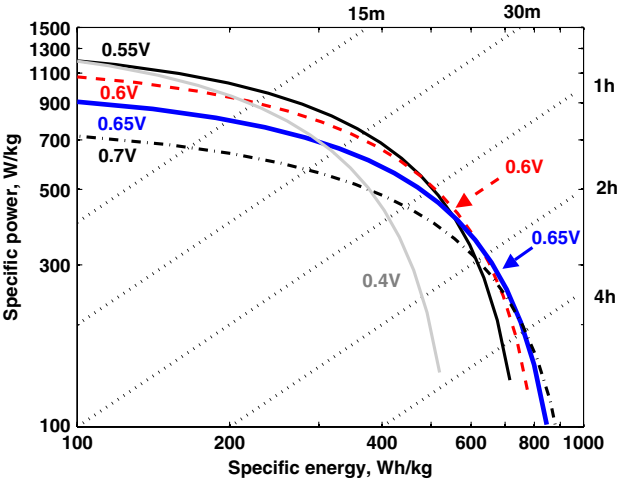


**Fig. 8 Specific power versus specific energy for various cell voltages (700 bar type-4 tanks).**

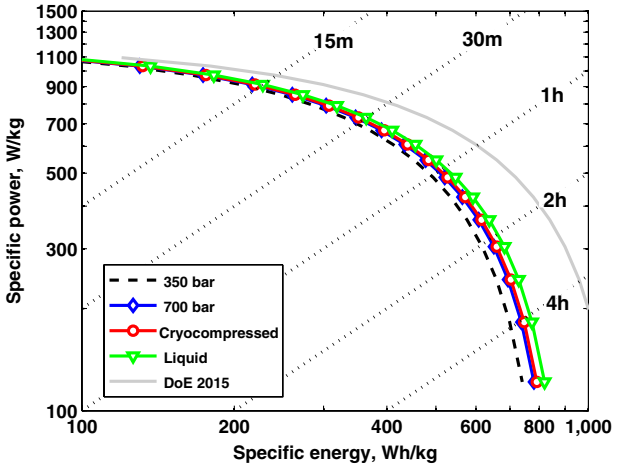


a) Specific power versus specific energy

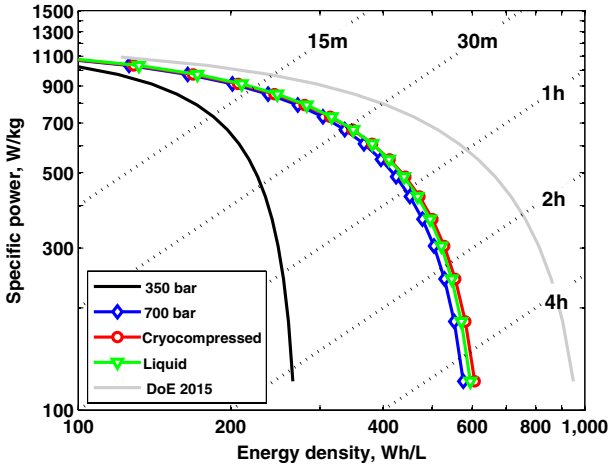


b) Specific power versus energy density

**Fig. 9 Effect of hydrogen storage technology; cell voltage 0.6 V.**

purposes. From Fig. 9b, it is obvious that, in terms of volume, 700 bar storage is far superior to 350 bar, beyond which all storage types coalesce again. Both figures appear to indicate that there is no significant advantage in using liquid hydrogen over 700 bar gaseous hydrogen with current technology. Thus, the additional cost of liquefaction and weight of cryogenic storage is best avoided at the power levels of present interest.

### C. Lithium-Ion Battery Pack

The lithium-ion model considers a discharge profile (under constant current) similar to that of Nissan Leaf-like cells, rated as (0.3 C) 33 Ah, as baseline (the notation means 33 Ah delivered when current drawn is $0.3\ \mathrm{C} = 0.3 \times 33 = 9.9$ A, where C denotes current of the same amount in A as capacity in Ah. It also means a corresponding discharge time of $1/0.3 = 3.33$ h). The discharge profiles at other currents are then found using an elementary battery model consisting of an incremental internal resistance and a Peukart coefficient that are set to reproduce available data at the other current levels (Fig. 10). A more refined battery model consisting of resistor–capacitor circuit elements [20] is considered beyond the scope for this conceptual design exercise. The Peukart coefficient and the internal resistance are set to $k = 1.01$ and $r = r_0(1 + If)$, where $r_0$ is a constant resistance, $I$ is the current in C (i.e., as a fraction of rated capacity), and $f$ is a factor that depends on the depth of discharge $x$, $f = 1 - \exp[-20x] - \exp[-20(1 - x)]$.

The state of the art in commercially available/custom made lithium-ion cells suitable for aviation ranges from 20 to 55 Ah capacities. Below 20 Ah, energy content is too low. Above 55 Ah, maximum current is limited. Consider some of the commercial off-the-shelf (COTS) lithium-ion cells available today. The data points

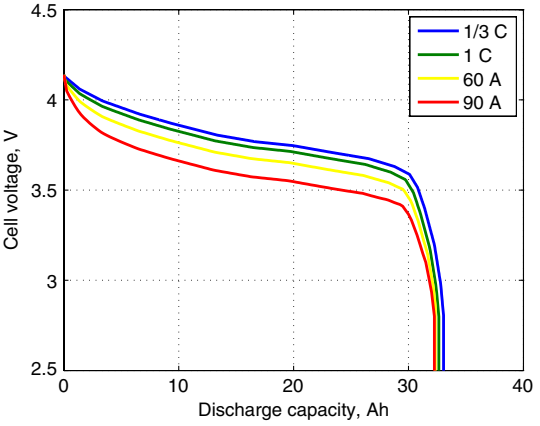


**Fig. 10 Simulated discharge profiles of (0.3 C) 33 Ah lithium-ion cells using an elementary battery model.**

include AESC (supplier of Nissan Leaf), LTC (supplier of Sikorsky Firefly), SAFT, A123, Winston, and Ping. As shown in Fig. 11a, the cell weights approximately track cell capacity. The cell voltages all lie nominally around 3.6 V, and so capacity is also a nominal measure of energy content. But, a high-capacity cell cannot simply be chosen and assumed to deliver the required power because the current must be restricted to within limits of continuous operation. This is a key restriction and implies that specific energy, not specific power, is the proper basis for design. The specific power and specific energy of these cells, within the restrictions of continuous current, are shown in Fig. 11b. Also shown is the Ragone plot of the fuel cell (the 0.65 V

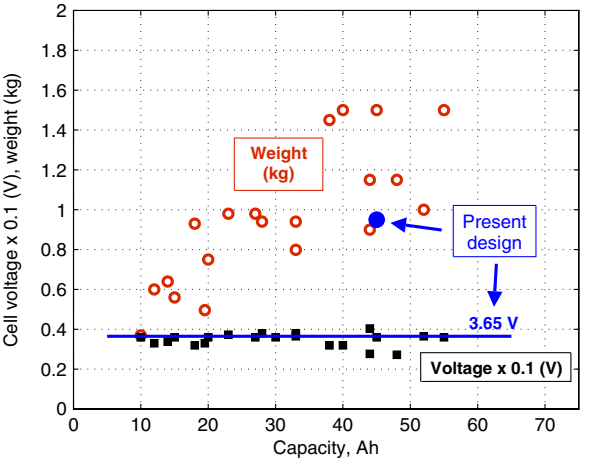


a) Cell weight and voltage versus capacity

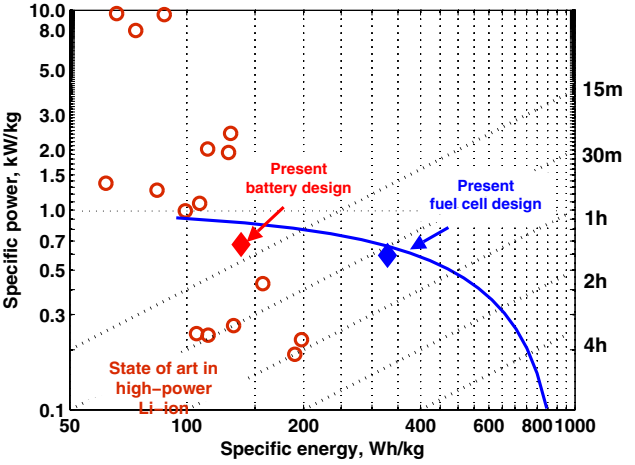


b) Cell specific power versus specific energy

**Fig. 11 State of the art in lithium-ion cells.**

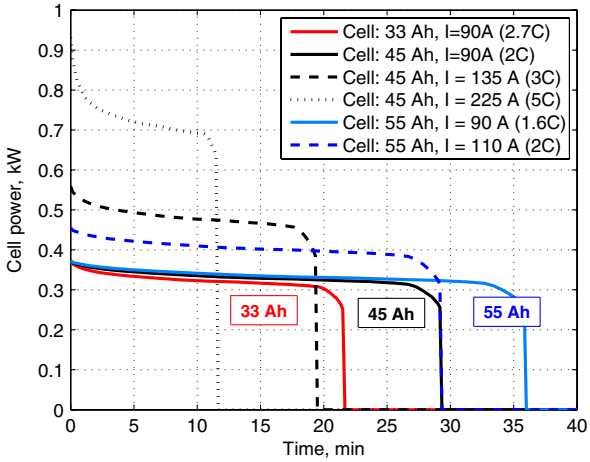


**Fig. 12 Various power profiles calculated using current technology high-power lithium-ion cells.**

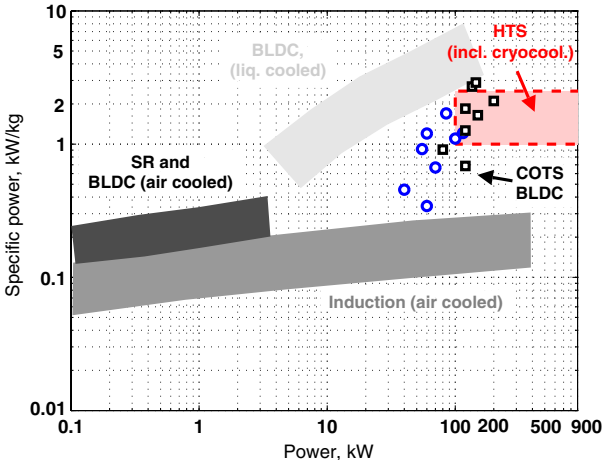


**Fig. 14 State of the art in electric motors applicable to EVs and HEVs.**



line from Fig. 8). It is clear that, for flights of less than 15 min, batteries are superior. But, for any practically useful endurance, fuel cells are required. Thus, this plot summarizes the basis for the benefits of hybridization. The design points for a 90 kg PL case (described later) are demarkated in the plot for reference.

Figure 12 shows the power profiles of several cells calculated by applying the battery model. From the Leaf cells operating at 90 A, the capacity is increased to include two other cells. The 45 Ah cells are taken up to 5 C (recommended continuous operation is up to 2 C). The 55 Ah cells have maximum continuous current rating of only 2 C. Figure 12 shows the maximum power that can be delivered by these high-energy cells. For example, it is clear that for 20 min of power assist, the 45 Ah cells will be the most appropriate if operated at 3 C. The 33 Ah cells would not last as long and the 55 Ah cells will not deliver as much power. Thus, not only improved capacity is required, but constructions that allow higher continuous current ratings are needed. For illustration, consider three cells rated 33, 45, and 55 Ah. If a battery were to be constructed that could deliver 30 kW over 12 min (up to 85% discharge), then their minimum weights are found to be 55, 40, and 33 kg with operation at 210, 150, and 122 V. The current drawn would vary 3.5–4.5 C and follow the profiles shown in Fig. 13. These currents are at the high end of what is potentially feasible today.

The volume is approximated as $(2.574 \times \text{capacity}/33)$ L/cell using Leaf dimensions (battery pack dimension of $1.571 \times 1.188 \times 0.265$ m for 192 cells) scaled by Leaf capacity of 33 Ah. This leads to very conservative energy density values.

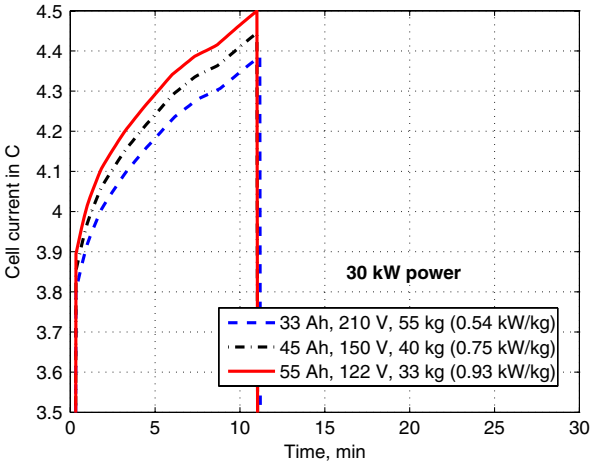


**Fig. 13 Cell current (in fraction of capacity value) to deliver 30 kW power for 12 min using three types of cells — 33, 45, and 55 Ah.**

### D. Electric Motor

The electric motors used in HEVs and EVs are primarily AC synchronous permanent magnet motors (EVs: Honda FCX and Clarity fuel cell cars, Nissan Leaf, Chevy Equinox fuel cell car, Chevy Sequel fuel cell car, etc.; HEVs: Chevy Volt, Nissan Tino, Honda Insight, Toyota Prius, etc.) or AC induction motors (EVs: Tesla, BMW Mini E, etc.). Some simple/early applications use DC motors (also popular for home-built EV conversions [21]) and some new applications explore switched reluctance motors, but their specific powers are too poor for any consideration for aviation. AC synchronous permanent magnet motors are the same as brushless DC (BLDC) motors (with sinusoidal stator winding, which is usually the case) except for the controller. These motors have the highest specific power in the power range of interest here.

The state of the art in electric motors is summarized in Fig. 14. The generic bands are taken from [22], with points added using motor, controller, and cooling system data from several manufacturers (where available), including U.S. Hybrid (Sikorsky Firefly supplier) and UQM (Boeing fuel cell airplane supplier). The specifications of a few motors in the required power range are shown in Table 6. Motor-6 appears marginally appropriate for the R 22 because it is capable of 85 kW of maximum continuous power compared to 93 kW of the original powerplant. A more suitable motor is Motor-7. This is capable of 100 kW of continuous power but is twice as heavy — 91 kg compared to 50 kg. It is assumed that a motor can be custom made to maintain similar size characteristics of Motor-6 — 1.7 kW/kg and 4.78 kW/L — so that, for 93 kW of maximum continuous power, the estimates are 54.7 kg and 19.5 L.

Over the last two decades, there have been significant research and development efforts in the area of high-temperature superconducting (HTS) machines (induction motors and generators) [23]. HTS motors are being introduced today for submarine applications of up to 35 MW of power. In aviation, studies have been conducted, beginning as early as two years after the discovery of HTS phenomena in 1985 (see [24] for a study including a heavy-utility CH-53 helicopter) to a more recent NASA/U.S. Department of Defense university program (see [25] for studies on Cessna 172 to notional heavy utility airplanes). HTS motors can provide more than twice the specific power of conventional induction motors (with potential for greater improvements) but, in the power range of interest in the present application (and below 1000 hp in general), limitations of scaling in the cryocooling system make them fall short of BLDC motors. An approximate band for such motors in the power range of interest is shown in Fig. 14.

Transmission requirements are unique in rotorcraft. The high-torque–low-rpm requirements for the helicopter rotor are an order of magnitude apart from high-torque–low-rpm operations of electric motors. Even the ultralight utility helicopter considered here operates around 2000 Nm and 510 rpm (rpm is nominally constant in helicopter rotors within ±5% variation), whereas the closest operation of the Honda Clarity 2009 motor is around 240 Nm and 4000 rpm at the rated power (maximum torque is 256 Nm). The

**Table 6 Commercially available motors having power ratings similar to those required for a hydrogen helicopter**

| Motor number | $P_{max/cont}$, kW | $Q_{max}$, Nm | Speed, rpm[d] | DC voltage, V | Weight, kg | Volume, L |
|---|---|---|---|---|---|---|
| 1[a] | 120/– | 1200 | 2500 | 250–700 | 95 | 64 |
| 2[a] | 120/– | 450 | 4500 | 250–700 | 65 | 29 |
| 3[b] | 80/40 | 250 | 5000 | 288 | 88 | 18.5 |
| 4[b] | 120/60 | 635 | 5000 | 288 | 175 | 39.8 |
| 5[c] | 135/60 | 340 | 3800 | 270–425 | 50 | 17.8 |
| 6[c] | 145/85 | 400 | 4000 | 340–420 | 50 | 17.2 |
| 7[c] | 150/100 | 650 | 3700 | 340–420 | 91 | 31 |
| 8[c] | 200/115 | 900 | 3500 | 340–420 | 95 | 32 |

[a]These numbers represent U.S. Hybrid motors.
[b]These numbers represent EV Tech motors.
[c]These numbers represent UQM motor generators (PowerPhase 135, 145, 150, and 200).
[d]This speed is the minimum value at which $P_{max}$ can be delivered.

engine rpm of the helicopter being 2652, use of such a motor can only increase the transmission weight. Motor-6, used as the basis for design here, has similar characteristics: the closest torque–speed operation is at 200 Nm and 4000 rpm at continuous power. The transmission weight is assumed to remain the same. For a new aircraft, the motor and transmission must be considered together.

## IV. Characteristics of the All-Electric Powerplant

The powerplant is sized to provide a maximum net power of 97.5 kWe at SL/ISA — the original engine maximum derated power. Three options are considered: a fuel-cell-only (FC-only) option, a battery-only (B-only) option, and a battery–fuel cell hybrid (BFC-hybrid) option. By options, primary power sources are meant; auxiliary power (for startup, onboard electrical systems, etc.) will always require some backup batteries.

### A. Powerplant Size

#### 1. *Fuel-Cell-Only Powerplant*

The FC-only powerplant consists of the S2.98 stack and corresponding C–E, hydrogen storage at 700 bar in a type 4 tank, and a BLDC motor. The weights of the components are shown in Tables 7 and 8. The motor and controller needed by the C–E uses Honeywell numbers [18,19] directly. The water management, thermal management, power electronics, and other accessory weights are estimates. The entire fuel cell system has specific power = 97.5 kW/150.2 kg = 0.65 kW/kg, and power density = 97.5 kW/144.16 L = 0.68 kW/L (note that 150.2 kg and 144.16 L are subtotals in Tables 7 and 8 minus electronics and drive). The DOE 2015 targets for affordable automobile fuel cell systems are 0.65 kW/kg and 0.65 kW/L. Including the fuel system (described later), the specific power reduces to 0.47 kW/kg and 0.41 kW/kg, for 2.58 and 4.12 kg hydrogen, respectively.

**Table 7 Weights and volume summary for an FC-only powerplant using high-end current technology[a]**

| Components | | Weight, kg | Volume, L |
|---|---|---|---|
| Fuel cell | Stack | 89.15 | 74.40 |
| | Accessories | 5.00 | 5.00 |
| Air | C–E | 27.55 | 16.26 |
| | Motor/controller | 6.50 | 8.50 |
| Water | Humidifier | 5.00 | 15.00 |
| | Condenser/tank | 2.00 | 5.00 |
| Heat | Exchangers | 4.50 | 3.00 |
| | Radiator | 7.50 | 15.00 |
| | Air cooler | 3.00 | 2.00 |
| Electronics | Control system | 2.00 | 2.00 |
| | Backup batteries | 3.00 | 3.00 |
| Drive | Motor | 54.70 | 19.50 |
| | Transmission | as is | as is |
| Subtotal | | 209.90 | 168.66 |

[a]Net power = 97.5/67.5 kWe (maximum/design). The two fuel levels correspond to 90 and 60 kg payloads, respectively.

For the original aircraft, the powerplant weight was 117 kg (manufacturer's engine dry weight only). That powerplant is now replaced with a new system of 209.9 kg. This is an increase of 92.9 kg and is also greater than the original powerplant and fuel system weights combined, by 7.9 kg. Thus, the new PL must be lower than the original. Tables 7 and 8 show the two fuel systems corresponding to 4.12 and 2.58 kg of hydrogen. These correspond to PL of 60 kg (unmanned) and 90 kg (manned), respectively. For a GTOW of 622 kg, the weights are summarized next.

Old empty weight − old powerplant − old tank = 388 − 117 −4 = 267 kg

For a manned/solo pilot option,

New empty weight = 267 + new powerplant + new tank for 2.58 kg hydrogen = 532 kg

Payload = GTOW − 532 = 90 kg

For an unmanned option,

New empty weight = 267 + new powerplant + new tank for 4.12 kg hydrogen = 561.9 kg

Payload = GTOW − 561.90 = 60.10 kg

A slightly greater PL of 109 kg (71% of original 153 kg maximum per seat weight, including baggage compartment) can be carried, but will require reducing the fuel system weight further down to 36.1 kg, which will allow only a meager 1.6 kg of hydrogen.

#### 2. *Battery-Only Powerplant*

Batteries are energy limited; therefore, specific energy is the proper basis for design. The approach followed is to specify a target weight and a maximum power, and then determine what specifications (capacity and configuration), constrained by the state of the art (weights and continuous current), maximize its time of operation. The target weight is set to be the same as the FC-only powerplant (minus electronics and drive system) for every PL. For example, for the 60 kg PL, the target weight is 205.3 kg corresponding to the FC-only system with 2.58 kg hydrogen. This design is shown in the first column of Table 9. It consists of 73 units in series with two cells in parallel in each unit. The battery management and cooling systems are assumed part of the cell overhead (0.6 kg/cell, based on Nissan Leaf).

#### 3. *Battery–Fuel Cell Hybrid Powerplant*

The approach followed in designing a battery for a BFC-hybrid powerplant is similar to that followed for designing the B-only

**Table 8 Weights and volume summary for hydrogen storage using high-end current technology**

| Fuel system | | Weight, kg | Volume, L | Weight, kg | Volume, L |
|---|---|---|---|---|---|
| | Hydrogen | 2.58 | In tank | 4.12 | In tank |
| | Tank/s | 47.52 | 66.50 | 75.88 | 106.19 |
| | Accessories | 5.00 | 2.00 | 5.00 | 2.00 |
| Subtotal | | 55.10 | 68.50 | 85.00 | 108.19 |
| Total | | 265.00 | 237.16 | 294.90 | 276.85 |

**Table 9 Three lithium-ion battery designs, BX.Y[a]**

| Specifications | Battery only B20.98 | BFC hybrid B8.30 | BFC hybrid B4.30 |
|---|---|---|---|
| Cell, Ah | (0.3 C) 45 | (0.3 C) 45 | (0.3 C) 19.5 |
| Number of units | 73 | 47 | 61 |
| Cells/unit | 2 | 1 | 1 |
| Cell weight, kg | 0.8 | 0.8 | 0.496 |
| Cell overhead, kg | 0.6 | 0.15 | 0.15 |
| Maximum power, kW | 97.5 | 30.0 | 30.0 |
| Discharge time, min | 12.5 | 13.0 | 7.2 |
| Voltage, V | 300–260 | 195–170 | 255–215 |
| Continuous current, C | 3.6–4.1 | 3.5–4.0 | 6.0–7.0 |
| Energy, Wh | 20.31 | 6.5 | 3.6 |
| Specific energy, kWh/kg | 0.100 | 0.146 | 0.091 |
| Specific power, kW/kg | 0.477 | 0.672 | 0.761 |
| Energy density, kWh/L | 0.040 | 0.039 | 0.039 |
| Weight, kg | 204.4 | 44.7 | 39.4 |
| Volume, L | 512.5 | 165 | 93 |

[a]*X* is nominal energy capacity in kWh and *Y* is maximum power in kW; units are in series, cells in an unit are in parallel; discharge time and energy are for 85% discharge at maximum power; operations correspond to SL/25°C.

powerplant except that a target duration of power assist is now specified instead of a target weight. The maximum power specified is 30 kW and the target durations are a minimum of 12 and 6 min, respectively (up to 85% discharge). These targets are obtained from the benchmark missions described in the next section, and are meant to use the battery for assist during hover only. The battery designs are designated B8.30 and B4.30 and are shown in columns 2 and 3 in Table 9 (8 and 4 are the nominal energy capacities to full discharge and 30 is the maximum power).

The fuel-cell powerplant is redesigned for a 30 kWe reduced maximum net power (down to 67.5 from 97.5 kWe earlier). This amounts to a simple linear scaling for the stack and C–E weight. The other BOP weights are also assumed to scale linearly. The power electronics weight is kept the same. The reduction in fuel-cell system weight is then around 45 kg.

A power of 30 kW delivered for 12 min (up to 85% discharge) means a nominal energy capacity of 6 kWh. A cell of capacity 45 Ah, maximum continuous current of 4 C, and weight less than 1 kg (including overhead) is a minimum requirement for keeping the total powerplant weight the same as the FC-only powerplant. This is more advanced than COTS technology today, but not infeasible. Cells with rating (0.3 C) 45 Ah, 2 C maximum continuous current, and weight 1.5 kg are possible today. The nominal voltage is 3.6 V, and so nominal cell capacity is 162 Wh, and nominal specific energy 0.108 kWh/kg. It is assumed similar cells can be obtained with 4 C maximum continuous current rating. Also, a reduced overhead is assumed. The cell weight is assumed the same as the Nissan Leaf cells, which are 0.8 kg/cell plus a packaging overhead of 0.6 kg/cell. But, because the required capacity is lower (6 kWh is 25% of the Leaf's capacity of 24 kWh), a proportionately reduced overhead of 0.15 kg/cell is assumed. Under these assumptions, B8.30 is obtained (Table 9). The specific power is then 0.672 kW/kg. This is slightly higher than the FC-only system. It weighs 44.7 kg, just about the same amount gained by reducing the fuel cell rating. Thus, there is no benefit in PL. But the same PL can now be carried over a greater range because the rate of fuel consumption will be lower in hover.

A power of 30 kW delivered for only 6 min (up to 85% discharge) means a capacity of only 3 kWh and enables a more easily achievable design with current state of the art. A COTS cell of capacity 19.5 Ah, maximum continuous current of 18 C, and of weight 0.496 kg can be found that is suitable for this purpose. Considering the same overhead of 0.15 kg/cell, the battery weight is now 39.4 kg (B4.30 in Table 9). This also provides a small increase in PL of 5.6 kg.

### B. Engine Charts

The typical engine characteristics needed for performance analysis are power versus altitude and power versus fuel flow. In turbo-shaft engines, there is a variation of power with speed (due to ram effect in the compressor), but this effect is nonexistent in piston engines, and also considered nonexistent here.

The engine charts are shown for the FC-only powerplant. This is because the loss of engine power with altitude is unavoidable and also the most severe for a fuel cell system. Batteries undergo severe deterioration of capacity at low temperatures, but this loss can be avoided with adequate heating. For the BFC-hybrid powerplant, the loss is from the fuel cell, but proportionately lower.

The engine charts are shown in Figs. 15 and 16. The power available with altitude (Fig. 15) is shown for a standard day and a 95° F day. The power available drops with altitude due to increasing C–E loss. As pressure drops with altitude, the compressor requires more power to keep the stack pressure constant at 2 atm. Without the stack pressure kept constant, the fuel cell will suffer dramatic losses — of the order of 5–20% in power — due to degradation of its characteristics (see Figs. 4a and 4b). If the stack pressure, temperature, and humidity are maintained, there should be no further loss with altitude. However, to be conservative, it is assumed that there still occurs an additional loss of 0.5% in power per 1000 ft, beyond 1000 ft. This means that, for a given cell current $i$, the cell voltage $v$ and power $p$ will drop by 0.5%. Figure 15 shows that this amount of loss is still significant, highlighting the importance of maintaining the stack operating conditions precisely.

The fuel flow required to deliver a net power (Fig. 16) is shown at two different altitudes — SL and 6000 ft. The maximum power in this

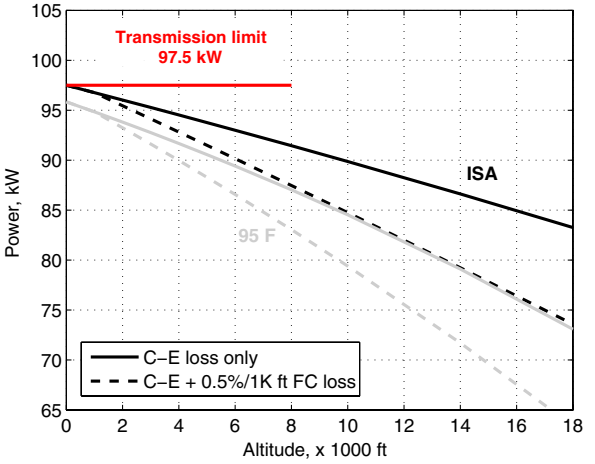


**Fig. 15 Maximum net power delivered versus altitude; ISA and 95°F (35°C). ("K" denotes ×1000 in all figures.)**

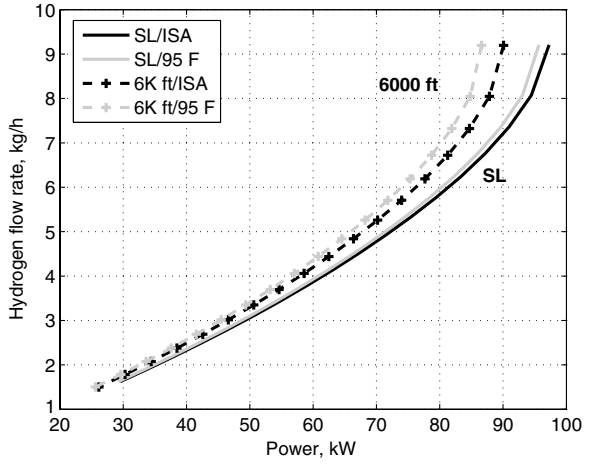


**Fig. 16 Hydrogen flow versus net power available; at SL and 6000 ft.**

plot are the values at SL and 6000 ft in Fig. 15. There is greater power increase with flow rate in the lower power regions; that is, an increase in power from 40 to 50 kW requires a 0.5 kg/h increase in flow rate, whereas an increase from 70 to 80 kW requires a 1 kg/h increase. This is simply a reflection of the individual cell characteristic curves (Fig. 4b).

## V. Performance of the All-Electric Helicopter

The aircraft and the powerplant models are now used to calculate the performance of the all-electric helicopter. The aircraft model calculates the power required for any gross weight, speed, altitude, and temperature. The powerplant model calculates the fuel flow required to supply a net power (after BOP expenses) at the same conditions. The performance analysis is limited to steady flight conditions using textbook procedures [26].

### A. Hover Performance

From power required to hover and the maximum power available at any altitude, the hover ceiling (highest altitude at which hover out of ground effect is possible) is calculated. Because altitude losses are the greatest for the FC-only powerplant, the hover performance is shown for this powerplant only.

The hover ceiling is shown in Fig. 17a. With a maximum GTOW of 622 kg, the helicopter can hover at only up to around 7200 ft on a standard day and at around 4900 ft on a hot 95°F day. Below these altitudes, the excess power can be used to climb. For a GTOW of 622 kg, the variation of steady rate of climb in hover with altitude is shown in Fig. 17b. The plots highlight the significant deterioration that can be caused by even a 0.5% loss in fuel cell power (per 1000 ft altitude gain). Even then, the hover performance is superior to the current piston engine aircraft. It is the duration of flight that is drastically diminished. This effect is felt predominantly in cruise performance, as illustrated next.

### B. Cruise Performance

All cruise performances are calculated using engine losses from both C–E and FC degradation. During cruise, the fuel cell alone is meant to provide the full power (corresponding to speed $V_{br}$), regardless of whether the powerplant is FC only or the BFC hybrid. The performance does depend on which powerplant is considered (near maximum power operation), but remains nominally the same. The payload range curves are, therefore, compared between the FC-only and B-only powerplants. In cruise, the BFC-hybrid curve will be similar to the FC-only curve.

The rate of climb in cruise is shown in Fig. 18a. Note that the value at zero speed is the initial rate of climb in hover. The steady rate of climb is twice this value, as shown in Fig. 17b. There is substantial drop in rate of climb with altitude and temperature below 80 kt speed due to substantial drop in engine power. The corresponding fuel flow required is shown in Fig. 18b. The fuel flow is almost proportional to the power required (see Fig. 16) at lower power but increases substantially at higher power. Conventionally, 1.05% of fuel flow is considered to account for engine degradation, but hydrogen being expensive and this being a specialty engine, that is not done here. Speed (km/h) divided by the fuel flow (kg/h) gives specific range (SR) (Fig. 18c), and the speed corresponding to maximum SR is the best range speed. Conventionally, the 99% of maximum SR on the higher speed side of the maximum is used to determine the best range speed. The SR varies with gross weight, and so, as fuel is burned (and exhaust water/vapor discarded) and gross weight reduces, SR increases. But this is a small effect for a hydrogen helicopter because the amount of fuel will always be 4–6 times lower compared to gasoline (due to its high calorific value and also the fuel cell's higher efficiency). The main weight is that of the storage tank, which cannot be discarded. Because of these reasons, the payload range curve is flat compared to a conventional fuel.

The payload–range curve at SL/ISA is shown in Fig. 19. Recall that the original payload cannot be flown at any fuel level. But 71% of the original payload can be flown (109 kg). This will allow only 1.6 kg of fuel, however, with which a distance (one way) of only 60 km can be covered. An important difference between the new hydrogen helicopter and the old conventional one is that carrying less fuel allows no meaningful increase in payload. The horizontal line of the payload–range curve is flat because the new fuel has a high energy content and, hence, the aircraft has a higher specific range. Because tank weight dominates fuel weight, the fuel system of a hydrogen helicopter is best designed based on a different paradigm. Depending on the mission, the proper size tank must be fit in during operation. More important than the payload range lines is the line that joins the ends of the full-tank range points. This line demarkates the tradeoff between payload and larger hydrogen storage. Similarly, the line joining the end points of the full discharge (up to 85%) range point for various battery-only powerplants is also shown. This line demarkates the tradeoff between payload and larger batteries. The horizontal lines of the battery-only powerplants are perfectly flat (because battery discharge does not reduce its weight) and are not shown. All batteries are made out of cells rated (0.3 C)45 Ah, but with the design specifications (number of units, cells/unit, and voltage) varied to generate progressively heavier batteries to keep payload comparable to the fuel cell system. The payload and range of the original helicopter are marked in the plot for comparison. Extrapolation of the hydrogen storage and battery lines suggests that only batteries have the potential to carry a payload close to the original, but with practically no range; whereas only fuel cells have the potential to fly a

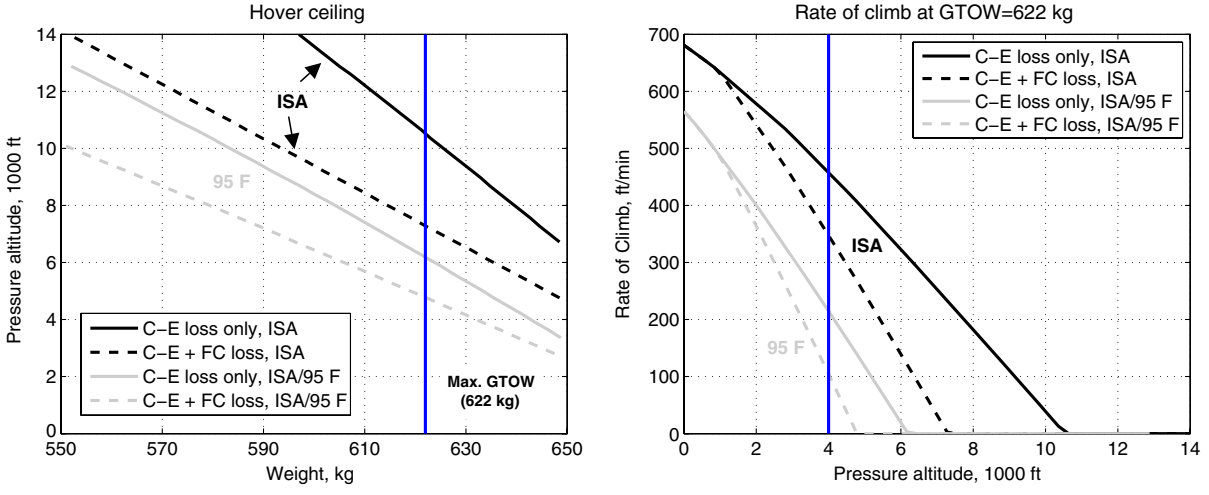


a) Hover ceiling b) Hover steady rate of climb for GTOW 622 kg

**Fig. 17 Hover performance; based on C–E loss only and C–E loss plus fuel cell degradation of 0.5%/1000 ft above 1000 ft.**

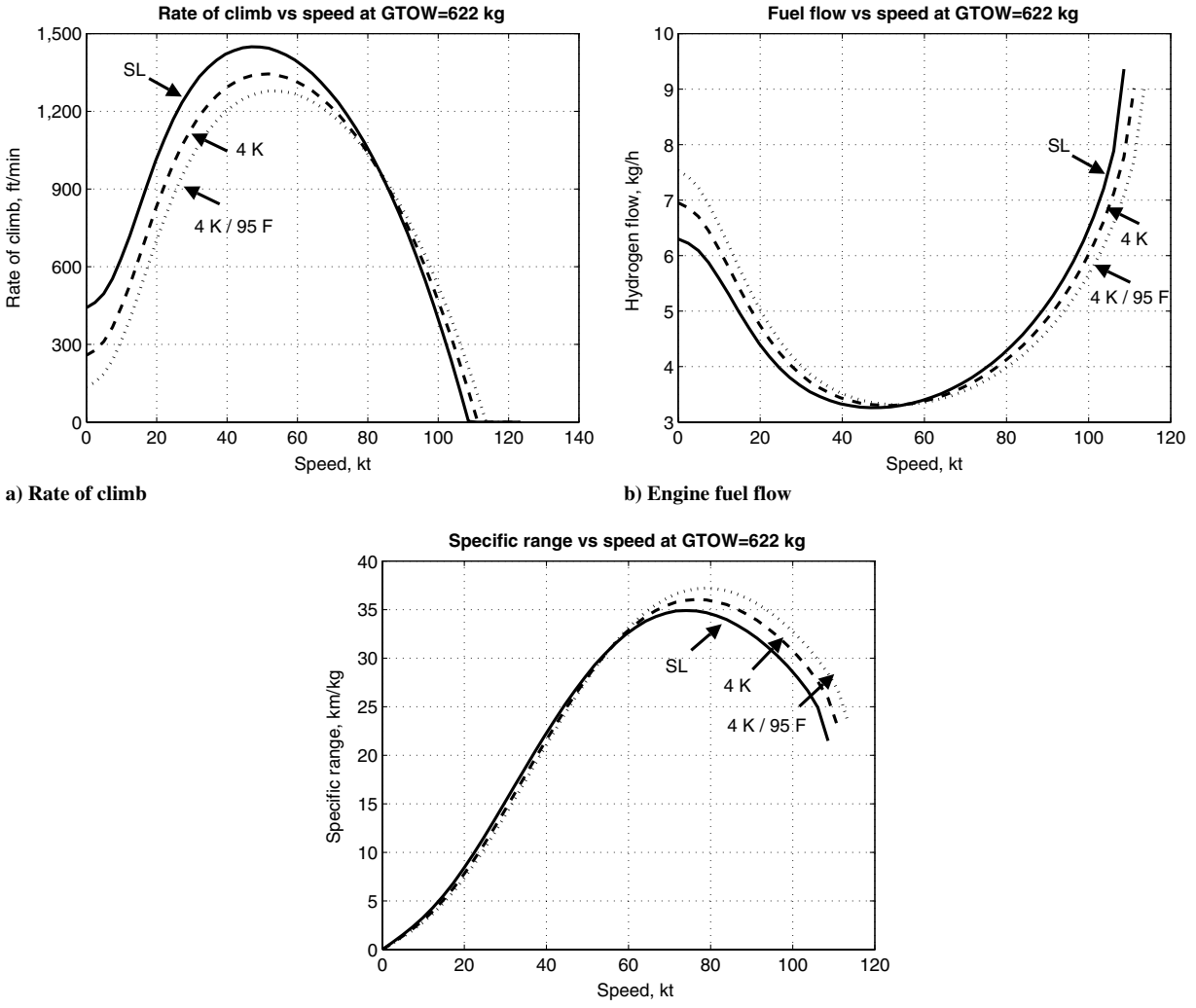


a) Rate of climb

b) Engine fuel flow

c) Specific range

**Fig. 18 Cruise rates of climb, fuel flows, and specific ranges for GTOW of 622 kg at SL/ISA, 4000 ft/ISA, and 4000 ft/95°F.**

range close to the original, but with practically no payload. The best solution today is clearly a combination of the two.

The range in the payload–range plot gives the maximum range possible under the ideal condition of continuous cruise at best range speed. For realistic range and duration of flight, a detailed mission analysis is required.

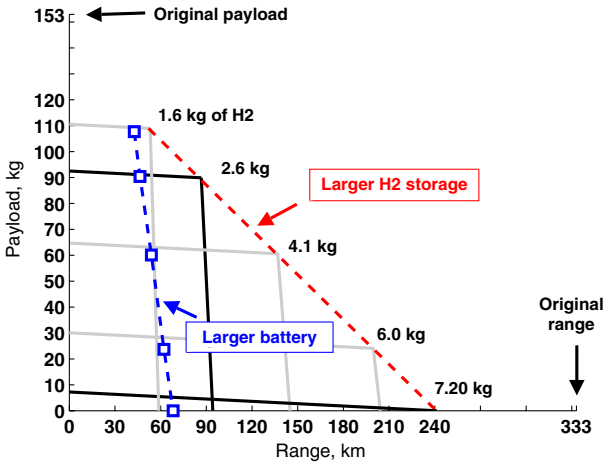


**Fig. 19 Payload versus range at SL/ISA with several fuel storage levels and battery weights.**

### C. Mission Analysis

*1. Three Benchmark Missions*

We propose three simple benchmark missions, as shown in Fig. 20. The first mission contains two segments of hover of 6 min total with cruise in between. The second mission begins with hover, is then followed by a climb to cruise altitude, then cruise at best range speed, followed by a descent at minimum power speed, and finally ends with hover. The hover segments, of 11 min total, are considered to be in moderately high/hot conditions. The climb, cruise, and descent are as per ISA. From hover to climb and then from descent to hover, it is assumed that conditions change abruptly between 3000/30°C and ISA. The cruise is in level flight — no gradual descent allowed. The descent has no range credit, and so is best done in minimum power speed. The third mission, at 4000 ft/95°F, does not have climb or descent segments. All missions contain takeoff and landing segments of 2 min each where thrust is assumed to be 50% GTOW.

*2. Performance with Battery-Only, Fuel-Cell-Only, and Battery–Fuel Cell Hybrid Powerplants*

The performance of the all-electric helicopter for the three benchmark missions is summarized in Table 10 for a nominal 90 kg PL case (solo pilot mission). Figure 21 shows the power profiles of the three missions. All missions carry an emergency backup of 0.38 kg of hydrogen (23–5% of total fuel corresponding to 1.6–7.2 kg of fuel). This corresponds to 3 min of hover at 3000/30°C or 13.8 min of cruise at 3000/ISA). These are not reserves in the conventional sense of the term but backups to cover for unforeseen losses. A mission is considered feasible only when a nonzero climb or cruise

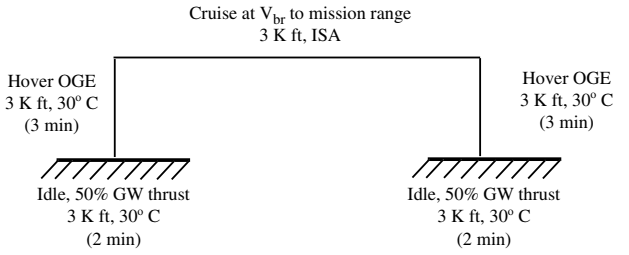


**a) Mission 1, simple**

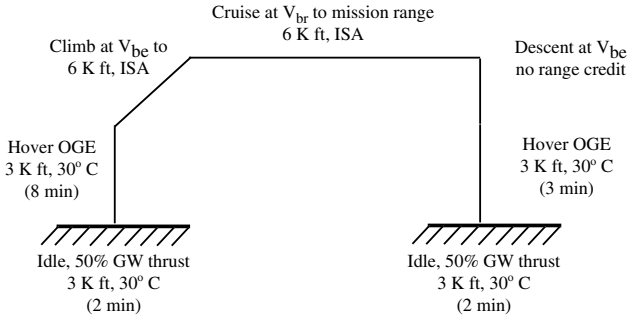


**b) Mission 2, nominal**

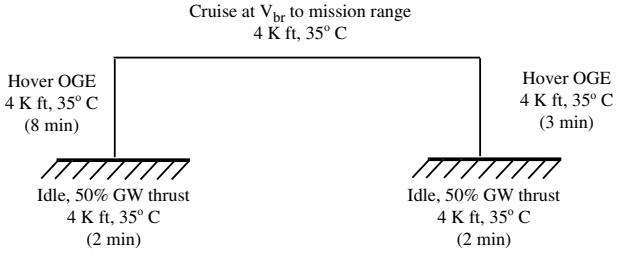


**c) Mission 3, hot/high**

**Fig. 20 Three missions for a light-utility manned all-electric helicopter.**

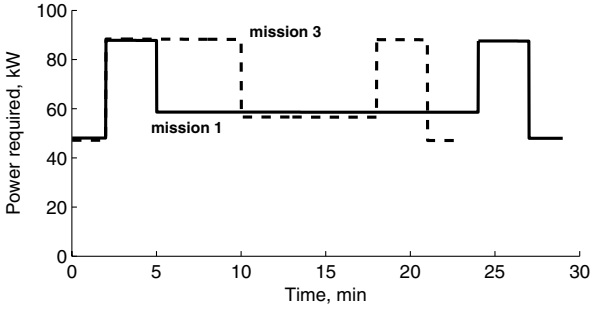


**a) Missions 1 and 3 (no climb)**

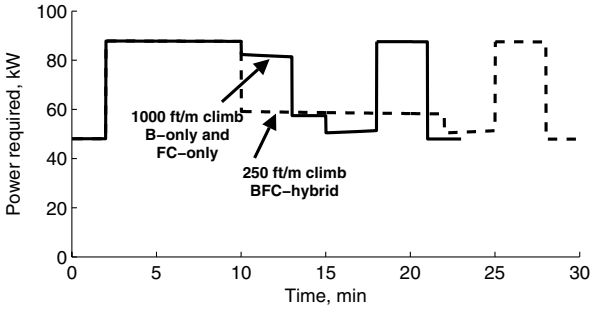


**b) Mission 2 (with climb)**

**Fig. 21 Power profiles of the three missions flown with 2.6 kg hydrogen tanks; 90 kg PL.**

segment is possible after takeoff/landing and hover requirements are met at both ends.

First, consider mission 1. With the B-only powerplant (using B20.98, Table 9), a total flight time of 10.17 min can be achieved (ignoring 4 min on ground). Out of these, 6 min are in hover, so the range is limited to only 9.7 km (4.17 min of cruise). With the FC-only powerplant, a total flight time of 25 min can be achieved with a range of 44.2 km. With the BFC-hybrid powerplant (using B4.30, Table 9), a total flight time of 30 min is possible with a range of 55.8 km. The PL is also increased slightly by 5.6 kg. Nonetheless, all three powerplants have poor performances. And given the variety of technology factors and assumptions that went into their design, it is premature to conclude that the FC-only powerplant is superior to the B-only powerplant. It is clear, however, that the BFC-hybrid is superior to both because the same technology factors and assumptions have gone into the hybrid.

Next, consider mission 2. Mission 2 has a climb segment. This mission cannot be flown with the B-only powerplant. The B-only powerplant, sized for the 90 kg PL mission (B20.98, Table 9), is effectively depleted due to requirements of hover at both ends. With the FC-only powerplant, the climb segment is flown at $V_{br}$ with a climb rate of 1000 ft/min. The power required during this segment is similar to that needed for hover. With the BFC-hybrid powerplant, this segment must be flown at a lower climb rate. The BFC-hybrid powerplant (using B8.30, Table 9) allows power assist for only 12 min. Hence, the powerplant can provide battery assist only in hover; during cruise, the fuel cell must provide the full power all by itself. The climb segment is, therefore, flown at $V_{be}$ to achieve the best climb rate. A climb rate of 250 ft/min can then be established, which means 12 min of climb to reach 6000 ft. The power profile, shown in Fig. 21b, is, therefore, different for this mission for the BFC-hybrid powerplant.

Now, consider mission 3. Even though hot and high, this mission has no climb segment. The B-only powerplant (B20.98, Table 9) again can barely make the mission. The general conclusion remains the same as before. The BFC-hybrid powerplant provides the best performance.

As a summary, the mission 3 payload versus range plot is shown in Fig. 22. This plot is different from Fig. 19 shown earlier in that it now corresponds specifically to mission 3; that is, it includes 11 min of hover. Only the lines that demarkate tradeoff between range and

**Table 10 Analyses of three missions with B-only, FC-only, and BFC powerplants[a]**

| Mission | Powerplant | Payload, kg | Fuel, kg | Range, km | Duration, min | Cruise time, min | Energy, kWh |
|---|---|---|---|---|---|---|---|
| 1 | B-only | 90 | | 9.7 | 14.2 | 4.2 | 20 |
| | FC-only | 90 | 2.6 | 44.2 | 29 | 19 | 31 |
| | BFC-hybrid | 95.6 | 2.6 | 55.8 | 34 | 24 | 36 |
| 2 | B-only | 90 | | – | – | – | 20 |
| | FC-only | 90 | 2.6 | 13.1 | 23.5 | 5.5 | 27 |
| | BFC-hybrid | 95.6 | 2.6 | 19.2 | 30 | 12 | 32 |
| 3 | B-only | 90 | | 1.6 | 15.7 | 0.7 | 20 |
| | FC-only | 90 | 2.6 | 19.2 | 23 | 8 | 27 |
| | BFC-hybrid | 95.6 | 2.6 | 47 | 34.6 | 19.6 | 32 |

[a]All missions have nominally 90 kg of payload and carry reserve fuel worth 3 min of hover at 3000/30°C or 13.8 min of cruise at 3000/ISA.

hydrogen storage or battery weight are shown. For the BFC-hybrid, the variation in PL is due to the variation in hydrogen storage. The advantage of using a hybrid system is now quantified. Because the hover duration is fixed and the battery is active only during hover, the curve corresponding to the BFC-hybrid powerplant shows a constant increment from the FC-only curve. The Boeing fuel cell airplane carried a solo pilot payload of 70 kg. At this level of payload, the hybrid powerplant can fly the aircraft to 90 km for a total duration of around 50 min.

## VI. Technology Status and Future Requirements

The technology status of the present all-electric powerplant is best described by locating it on the state of the art in rotorcraft engines (taken from [27]), modified into a form suitable for comparison. The brake specific fuel consumption (BSFC) and specific power (SP) are suitable measures for comparing piston/turbo-shaft engines. Because the fuel is different here, instead of BSFC, the fraction of fuel calorific value extracted by the engine is compared. This is denoted as efficiency of fuel consumption (EFC) and defined as

$$\text{EFC} = \frac{1/\text{BSFC}}{\text{fuel calorific value}} \tag{5}$$

The calorific values are 13 kWh/kg for gasoline and 39 kWh/kg for hydrogen. The EFC is applicable only to the fuel cell powerplant and corresponds here to a GTOW of 622 kg.

The efficiencies and specific power are shown in Figs. 23a and 23b, respectively. The increased efficiency of a fuel cell is clear from Fig. 23a. The value of BSFC, hence EFC, depends on the power level (because fuel flow depends on power level). The EFC is shown for two levels, one for maximum power (lower EFC) and the other for cruise power (higher EFC).

**Table 11 Technology levels for all-electric propulsion system used in present study, near term, and long term requirements**

| Technology | Present | Midterm (2020) | Long term (2030) |
|---|---|---|---|
| *Fuel cell stack* | | | |
| Cell $i_c$, $v_c$, A/cm$^2$-V | 0.35, 0.65 | 0.6, 0.75 | 0.7, 0.8 |
| Specific power (with BOP), kWe/kg | 0.65 | 1.5 | 3.0 |
| Power density (with BOP), kWe/L | 0.68 | 1.0 | 2.0 |
| *Compressor–expander* | | | |
| Flow rate, kg/s | 0.11 | 0.20 | 0.30 |
| Specific power, kW/kg | 0.65 | 2.0 | 3.0 |
| Power density, kW/L | 1.0 | 1.0 | 1.5 |
| Efficiency | 0.6 | 0.8 | 0.85 |
| *Hydrogen storage* | | | |
| $H_2$ gas, wt % | 0.054 | 0.075 | 0.15 |
| $H_2$ gas volume, kg/L | 0.038 | 0.04 | 0.04 |
| $H_2$ liquid, wt % | 0.055 | 0.075 | 0.15 |
| $H_2$ liquid volume, kg/L | 0.04 | 0.055 | 0.07 |
| Amount, kg | 4–5 | 7–10 | 10–15 |
| *Battery* | | | |
| Capacity, Ah | 20–45 | 55–75 | 100 |
| Maximum continuous current, C | 3–5 | 5 | 5 |
| Specific power, kW/kg | 0.7 | 2.5 | 5.0 |
| Specific energy, kWh/kg | 0.10–0.15 | 0.2–0.3 | 0.5 |
| Energy density, kWh/L | 0.04 | 0.25 | 0.5 |
| *Electric motor* | | | |
| Specific power (continuous), kW/kg | 1.7 | 2.5 | 4.0 |
| Power density (continuous), kW/L | 4.8 | 5.0 | 5.0 |
| Efficiency | 0.93 | 0.95 | 0.95 |
| Minimum speed, rpm | 4000 | 2000 | 1000 |
| Specific torque, Nm/kg | 4 | 12 | 38 |

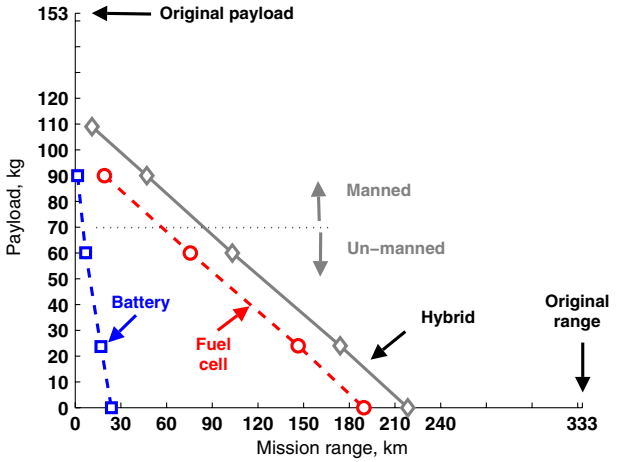


**Fig. 22 Mission 3 payload and range compared between the three powerplants.**

The poor state of specific power (Fig. 23b) is not surprising. The specific power of the original piston engine is at best 108/117 = 0.92 kW/kg (108 kW is maximum power before derated and 117 kg is the engine dry weight). This value lies near those achieved by helicopter piston engines since as early as 1940s–1950s and is similar to automobile engine state of the art in specific power. Basing the design on component technologies that are beginning to compete with automobile state of the art is expected to produce such a result. Clearly, the gap in the value of specific power is considerable to bridge. But, it forms a quantitative basis for setting requirements to bridge the gap.

Table 11 proposes a set of technology targets that are to be met if electric powerplants are to deliver or exceed the performance of piston engines (midterm, 2020) and turboshaft engines (long term, 2030). The DOE 2015 specific power target of 0.65 kWe/kg for the fuel cell stack is too low for aviation. For example, even if the specific power of the electric motor is increased to 2.5 kW/kg (considered

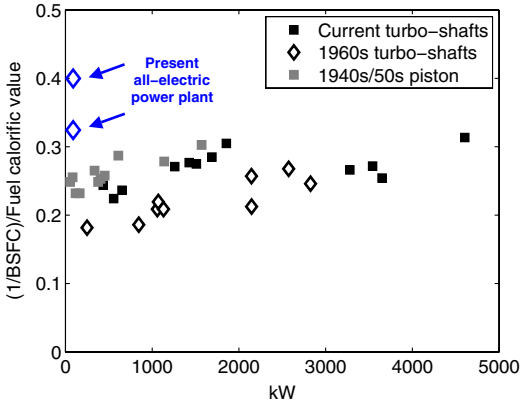


a) Efficiency normalized with fuel calorific value

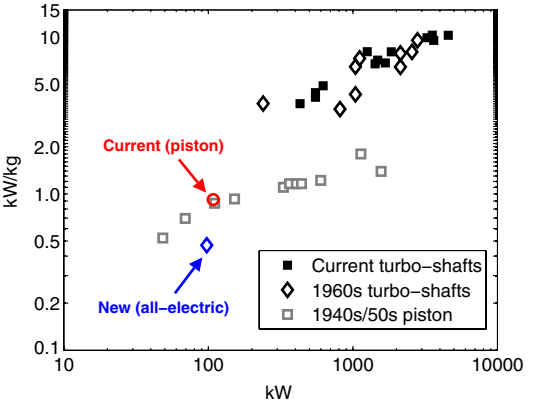


b) Specific power

**Fig. 23 Comparison of the new all-electric engine with the state of the art in rotorcraft combustion engines.**

2020 target), the specific power of the fuel cell stack must at least be 1.5 kWe/kg (considered 2020 target) so that the net powerplant specific power reaches 0.92 kW/kg, comparable to a piston engine. Such specific power may demand high-pressure operation, in which case the compressor–expanders must be designed accordingly to handle greater flow rates. Even greater targets are required to achieve performance closer to turboshaft engines (in the 500–1000 kW power range) or cover for weight penalty in gaseous hydrogen storage. For hydrogen storage, the DOE's ultimate wt % target of 0.075 must be met, and then exceeded toward 0.15. The DOE 2015 target of 0.055, currently achievable (regardless of cost), is not adequate. For example, assuming piston engine efficiency of 25%, 81 kg of gasolene (fuel weight of the R 22 Beta II) translates into 15 kg of hydrogen with the current design. Even if the fuel cell efficiency increases to 55% (0.8 V operation), 12 kg of hydrogen will still be required. Carrying this amount of hydrogen in a tank whose weight more than offsets the original fuel system weight diminishes the impact of using hydrogen. (This is somewhat more of a challenge in the ultralight utility range because plastic tanks used on such aircraft are hard to beat.) A special requirement for rotorcraft is a higher torque, lower rpm operation of the electric motor. If the minimum rpm (at which the maximum continuous power can still be delivered) can be lowered, significant weight savings from transmission can be achieved. Direct drives to rotors can eliminate the transmission altogether. But, a direct drive implies a high specific torque, numbers that can at present be delivered only by HTS motors operating at very high power (in mega-watts range). Thus, some of amount of gear reduction may always be required for conventional rotorcraft in the near future.

## VII. Conclusions

This paper described the conceptual design of three all-electric powerplants — a battery-only powerplant, a fuel-cell-only powerplant, and a battery–fuel-cell-hybrid powerplant — for use in a manned ultralight utility helicopter. The state of the art in component technologies was assessed, powerplant models were synthesized, a systematic evaluation of performance was carried out in hover and cruise, and technology targets were identified to achieve performance at par with internal combustion engines. Three benchmark missions were proposed for the analysis of all-electric rotorcraft. The electric powerplants were compared with each other and with the state of the art in present-day combustion engines. Technology targets were proposed to bridge the gap in future. Based on this study, four main conclusions are drawn. Note that these conclusions are to be considered in the context of an ultralight utility helicopter considered herein.

1) If a combination of the highest-end automobile EV technologies are brought to bear on aviation, the status of specific power will now be approximately one-half of the rotorcraft piston engines of comparable power. However, fuel efficiency will be higher by 50% to twice that of piston engines. Another main drawback for the entire propulsion system is the weight of the hydrogen tank. In the context of rotorcraft, gravimetric storage capacity (wt%) appears a far greater concern than volumetric storage capacity.

2) Batteries are superior for hover ceiling with adequate temperature control. Fuel cells are superior for cruise range with adequate pressure control. A combination of the two, with fuel cells sized for cruise and batteries sized for power assist during hover, appears to be the optimum solution with current technology (what was carried out by the Boeing fuel cell demonstrator, at a low power level, in the context of climb and cruise carries over to rotorcraft, but in the context of hover and cruise.)

3) For the R 22 Beta II helicopter, maintaining the same hover ceiling under SL/ISA means the original payload can no longer be flown. But, 60% of the original payload (90 kg) can be flown as a solo pilot option, and the best flight duration and range under these conditions are approximately 35 min total, including 11 min hover (plus 3 min worth of hover reserve) and 45 km range under high/hot (4000 ft/95°F) conditions.

4) An unique barrier to all-electric propulsion in rotorcraft is its high torque, low rpm rotor operation. This is different, by an order of magnitude, from what is considered high torque, low rpm in electric motors. For example, for the R 22 Beta II-like helicopter, torque–rpm is approximately 2000 Nm–510 whereas the Honda Clarity 2009 electric motor can operate at most at 250 Nm–4000 at the rated power. The transmission is an unique and major component in rotorcraft and, as such, offers a unique opportunity. One effective way to bypass the heavy powerplant and hydrogen tank will be to design an innovative drive that removes/reduces the need/weight for a transmission.

At the end, we note that the present design was constrained by the existing configuration, rotor system, airframe, and transmission. An integrated design of a new configuration, scaled to the new laws of fuel, motor, and tank weights, can be expected to provide modest improvements in performance. But, dramatic improvements can only be achieved if the core deficiencies of the powerplant are addressed.

## References

[1] International Energy Agency, "Electric and Plug-in Hybrid Electric Vehicles Roadmap," Directorate of Sustainable Energy Policy and Technology (SPT), Paris, June 2011.

[2] "FY2010 Progress Report For the DOE Hydrogen Program," U.S. Dept. of Energy DOE/GO-102011-3178, Feb. 2011.

[3] Lapeña-Rey, N., Mosquera, J., Bataller, E., Ortí, F., Dudfield, C., and Orsillo, A., "Environmentally Friendly Power Sources for Aerospace Applications," *Journal of Power Sources*, Vol. 181, No. 2, 2008, pp. 353–362. doi:10.1016/j.jpowsour.2007.11.045

[4] Lapeña-Rey, N., Mosquera, J., Bataller, E., and Ortí, F., "First Fuel-Cell Manned Aircraft," *Journal of Aircraft*, Vol. 47, No. 6, 2010, pp. 1825–1835. doi:10.2514/1.42234

[5] Chretien, P., "The Quest for the World's First Electric Manned Helicopter Flight," *Vertiflite*, Vol. 58, No. 2, March–April 2012, pp. 38–42.

[6] Schneider, D., "Helicopters Go Electric," *IEEE Spectrum*, Vol. 49, No. 1, Jan. 2012, pp. 11–12. doi:10.1109/MSPEC.2012.6117817

[7] Oyama, S., Kaji, H., and Yoshida, H., "Development of Honda FCX," *World Electric Vehicle Journal*, Vol. 2, No. 3, 2008, pp. 18–22.

[8] Matsunaga, M., Fukushima, T., and Ojima, K., "Powertrain System of Honda FCX Clarity Fuel Cell Vehicle," *24th International Battery, Hybrid and Fuel Cell Electric Vehicle Symposium*, Stavanger, Norway, May 2009.

[9] Durkee, S. R., and Muetze, A., "Conceptual Design of an Electric Helicopter Powertrain," *5th Institution of Engineering and Technology International Conference on Power Electronics, Machines and Drives*, Brighton, England, U.K., April 2010.

[10] Wood, P., and Muetze, A., "Conceptual Design of a Direct Helicopter Energy Storage System," *6th Institution of Engineering and Technology International Conference on Power Electronics, Machines and Drives*, Bristol, England, U.K., March 2012.

[11] Johnson, W., *Helicopter Theory*, Dover, New York, 1994.

[12] Datta, A., and Chopra, I., "Validation and Understanding of UH-60A Vibratory Loads in Steady Level Flight," *Journal of the American Helicopter Society*, Vol. 49, No. 3, 2004, pp. 271–287. doi:10.4050/JAHS.49.271

[13] "R22 Pilot's Operating Handbook and FAA Approved Rotorcraft Flight Manual," RTR-061, Robinson Helicopter Co., Torrance, CA, Dec. 2009.

[14] Barbir, F., *PEM Fuel Cells Theory and Practice*, Elsevier, New York, 2005, pp. 115–204.

[15] Spiegel, C. S., *Designing and Building of Fuel Cells*, McGraw–Hill, New York, 2007, pp. 247–311.

[16] O'Hayre, R., Cha, S., Colella, W., and Prinz, F. B., *Fuel Cell Fundamentals*, 2nd ed., Wiley, Hoboken, NJ, 2009, pp. 195–222, 331–451.

[17] Yan, Q., Toghiani, H., and Causey, H., "Steady State and Dynamic Performance of Proton Exchange Membrane Fuel Cells (PEMFCs) Under Various Operating Conditions and Load Changes," *Journal of Power Sources*, Vol. 161, No. 1, 2006, pp. 492–502. doi:10.1016/j.jpowsour.2006.03.077

[18] Gee, M. K., "Cost and Performance Enhancements for a PEM Fuel Cell Turbocompressor," *Proceedings of Hydrogen and Fuel Cells Program Annual Merit Review*, U.S. Department of Energy, May 2005.

[19] Ordonez, G., Gee, M. K., and Liu, C., "Air, Water and Thermal Management for PEM Fuel Cell Systems," *Fuel Cell Seminar*, San Antonio, TX, Nov. 2004.

[20] Chen, M., and Rincon-Mora, G. A., "Accurate Electrical Battery Model Capable of Predicting Runtime and *I-V* Performance," *IEEE Transactions on Energy Conversion*, Vol. 21, No. 2, June 2006, pp. 504–511.
doi:10.1109/TEC.2006.874229

[21] Warner, M., *The Electric Vehicle Conversion Handbook*, Penguin Putnam, New York, 2011, pp. 31–55.

[22] Larminie, J., and Lowry, J., *Electric Vehicle Technology Explained*, John Wiley & Sons, Ltd., West Sussex, England, U.K., 2003, pp. 141–181.

[23] Schiferl, R., Flory, A., Livoti, W. C., and Umans, S. D., "High-Temperature Superconducting Synchronous Motors: Economic Issues for Industrial Applications," *IEEE Transactions on Industry Applications*, Vol. 44, No. 5, 2008, pp. 1376–1384.
doi:10.1109/TIA.2008.2002219

[24] Turney, G. E., Luidens, R. W., Uherka, K., and Hull, J., "Aeronautical Applications of High-Temperature Superconductors," NASA TM-102311, 1989; also *Aircraft Design, Systems and Operations Conference*, AIAA Paper 1989-2142, July–Aug. 1989.

[25] Luongo, C. A., Masson, P. J., Nam, T., Mavris, D., Kim, H. D., Brown, G. V., Waters, M., and Hall, D., "Next Generation More-Electric Aircraft: A Potential Application for HTS Superconductors," *IEEE Transactions on Applied Superconductivity*, Vol. 19, No. 3, 2009, pp. 1055–1068.
doi:10.1109/TASC.2009.2019021

[26] Prouty, R. W., *Helicopter Performance, Stability, and Control*, Krieger, Malabar, FL, 2005, pp. 273–336.

[27] Rosen, K. M., "A Prospective: The Importance of Propulsion Technology to the Development of Helicopter Systems with a Vision for the Future, The 27th Alexander A. Nikolsky Lecture," *Journal of the American Helicopter Society*, Vol. 53, No. 4, 2008, pp. 307–337.
doi:10.4050/JAHS.53.307

A. Gallimore
*Associate Editor*